Soluble VCAM-1 May Serve as a Pharmacodynamic CSF Marker to Monitor BACE2 Activity in Non-Human Primates

Authors

Sarah K. Tschirner, Y. Joy Yu Zuchero, Jennifer A. Getz, Stephan A. Müller, Karsten Nalbach, Matthew E. Kennedy, Joseph W. Lewcock, and Stefan F. Lichtenthaler

Correspondence

Stefan.Lichtenthaler@dzne.de

In Brief

BACE1 inhibition is a tempting strategy to prevent Aβ accumulation in the brain, the key feature of Alzheimer's disease pathology. However, current small-molecule BACE1 inhibitors exhibit unwanted co-inhibition of BACE2, which is a possible reason for adverse effects. Using CSF proteomics, we identified soluble VCAM-1 as a cleavage product of BACE2 but not BACE1. Soluble VCAM-1 may thus serve as a biomarker to monitor BACE2 inhibition in future clinical trials for the development of new, BACE1-selective inhibitors.

Graphical Abstract

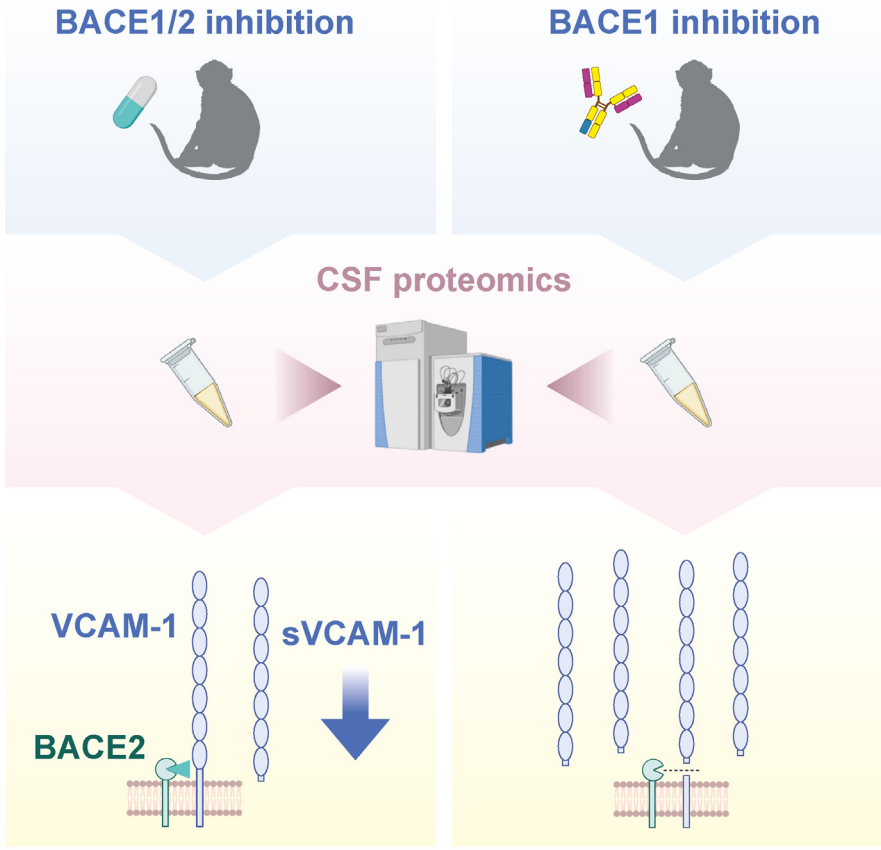

Highlights

- VCAM-1 is identified as a BACE2-specific substrate in the brain of non-human primates.
- Soluble VCAM-1 may serve as a biomarker to measure BACE2 target engagement in CSF.
- Soluble VCAM-1 measurement may help to control side effects in Alzheimer trials.
- Specific inhibition of BACE1 in the brain induces a specific proteome signature in CSF.

2025, Mol Cell Proteomics *24*(*7*), 101012

https://doi.org/10.1016/j.mcpro.2025.101012

Soluble VCAM-1 May Serve as a Pharmacodynamic CSF Marker to Monitor BACE2 Activity in Non-Human Primates

Sarah K. Tschirner[1,2], Y. Joy Yu Zuchero[3], Jennifer A. Getz[3], Stephan A. Müller[1,2], Karsten Nalbach[1,2], Matthew E. Kennedy[4], Joseph W. Lewcock[3], and Stefan F. Lichtenthaler[1,2,5,*]

The β-secretase β-site APP cleaving enzyme 1 (BACE1) is a major drug target for Alzheimer's disease (AD). Clinically tested BACE1 inhibitors induced unexpected cognitive side effects that may stem from their cross-inhibition of the homologous protease BACE2. Yet, little is known about BACE2 functions and substrates *in vivo*, and no biomarker is available to monitor the extent of BACE2 inhibition *in vivo*, particularly in cerebrospinal fluid (CSF). To identify a potential CSF biomarker for monitoring BACE2 activity, we analyzed the CSF proteome changes in non-human primates after treatment with a BACE1-selective inhibitor (a brain-targeted monoclonal antibody) in comparison to verubecestat, a clinically tested small-molecule drug inhibiting both BACE1 and BACE2. Acute treatment with either the antibody or verubecestat similarly reduced CSF abundance of the cleavage products of several known BACE1 substrates, including SEZ6, gp130, and CACHD1, demonstrating similar target engagement *in vivo*. One CSF protein, vascular cell adhesion protein 1 (VCAM-1), was only reduced upon inhibition with verubecestat, but not upon BACE1-selective inhibition with the antibody. We conclude that VCAM-1 is a promising biomarker candidate for monitoring BACE2 inhibition in CSF, which is instrumental for the development of BACE1-selective inhibitors for the prevention of AD.

Alzheimer's disease (AD) is a fatal, neurodegenerative disorder and the most prevalent type of dementia (1). While first immunotherapies are available to slow the disease course (2), neither curative nor preventive therapeutic strategies are available, making AD one of the most serious health concerns of this century (1).

Symptom onset is preceded by an up to 25-year-long preclinical state. A key event early in AD pathophysiology is the accumulation of Aβ aggregates in the brain (1, 3). The Aβ peptide results from proteolytic processing of the amyloid-β precursor protein (APP) first by the protease β-site APP cleaving enzyme 1 (BACE1) and then by γ-secretase (4, 5). BACE1-targeted small-molecule inhibitors were tested in advanced clinical trials to lower Aβ burden (3, 6). However, despite excellent target engagement and a successful reduction of Aβ in cerebrospinal fluid (CSF) and amyloid plaques in the brain of the participants, the trials were terminated prematurely (6). For most inhibitors, one major reason was the occurrence of mild cognitive worsening (6), at least partially accompanied by hippocampal shrinkage (7–9). Although the effects on cognition were non-progressive and, after treatment cessation, turned out to be reversible, further drug development needs to achieve the avoidance of such adverse effects (6).

Clinically tested BACE inhibitors do not exclusively block BACE1 but also, and in some instances even more potently, inhibit BACE2 (6), a close homolog of BACE1. This raises the possibility that the cognitive worsening side effect results from BACE2 inhibition and consequently the reduced cleavage of physiological BACE2 substrates (4, 6). BACE1 and BACE2 substrates are transmembrane and GPI-anchored membrane proteins. Upon cleavage within their extracellular juxtamembrane domain, the substrate's ectodomain is released into the extracellular space or body fluids. This proteolytic process is generally referred to as ectodomain shedding and controls the function and abundance of membrane proteins (10). While numerous membrane proteins were identified as BACE2 substrate candidates *in vitro* (11), only three proteins were demonstrated to require BACE2 cleavage to modulate their physiological function: PMEL in pigmentation (12), TMEM27 in pancreatic homeostasis (13, 14) and vascular endothelial growth factor receptor 3 (VEGFR3) in lymphatic vessel growth and maintenance (15). BACE2 is expressed in various peripheral tissues (16), including in melanocytes, where BACE2 activity supports melanoma proliferation (17), and also in the brain, including parts of the hippocampus (16, 18). Under certain conditions, such as in the case of APP mutations or binding to clusterin (19), BACE2 may cleave APP at the same peptide bond as BACE1 and contribute to Aβ

From the [1]German Center for Neurodegenerative Diseases (DZNE), Munich, Germany; [2]Neuroproteomics, School of Medicine and Health, TUM University Hospital, Technical University of Munich, Munich, Germany; [3]Denali Therapeutics Inc., South San Francisco, California, USA; [4]Neuroscience, Merck & Co. Inc., Boston, Massachusetts, USA; [5]Munich Cluster for System Neurology (SyNergy), Munich, Germany
*For correspondence: Stefan F. Lichtenthaler, Stefan.Lichtenthaler@dzne.de.

https://doi.org/10.1016/j.mcpro.2025.101012

generation (20). BACE2 expression is also increased in aged mouse brains (19). Yet, BACE2 also acts as an alternative α-secretase, cleaving APP within the Aβ sequence (21), and thereby counteracting Aβ pathology (20). BACE2 triplication in trisomy 21 was found to be protective against AD pathology in trisomy 21 cerebral organoids (21). Moreover, in patients with AD, lower expression levels of BACE2 were detected in the brain vascular system (22), where BACE2 may have a protective vascular function (23, 24). Thus, while the beneficial and detrimental functions of BACE2, including in the brain, in AD, and APP processing, are not fully understood, a specific inhibition of BACE1, but not BACE2, is desirable, for example, with small molecule drugs or BACE1-targeting antibodies (6, 25). Development of such drugs for clinical tests requires the ability to measure target engagement of BACE1 and BACE2 *in vivo*. While this is well established for BACE1, *e.g.*, using Aβ or some of the known BACE1 substrate cleavage products (15, 26–28), a suitable biomarker for BACE2 target engagement is lacking and remains a key challenge to be identified, in particular for CSF. In mice, the function of BACE2 in pigmentation is used to monitor BACE2 inhibition by depigmentation of chest hair regrowth, but this requires prolonged BACE2 inhibition of 2 weeks or more (15). Measuring BACE2 inhibition is currently not possible in non-human primates (NHPs), which are often used for the development of brain-targeting drugs (29), including in AD, as well as in humans. A BACE2 cleavage product of a recently identified BACE2 substrate, VEGFR3, may serve as a biomarker for BACE2 activity in mice, NHPs, and humans (15), but the assay needs to be improved for clinical utility and is restricted to plasma and not suitable for CSF, where the substrate was not detected.

To identify a potential CSF biomarker for monitoring BACE2 activity, we analyzed the CSF proteome changes of NHPs after treatment with a brain-targeted monoclonal antibody that demonstrates BACE1-selective inhibition (25) in comparison to verubecestat, a clinically tested small-molecule drug that inhibits both BACE1 and BACE2 (7, 8, 26). One protein, vascular cell adhesion protein 1 (VCAM-1), was identified and validated to be reduced only upon inhibition with verubecestat but not upon BACE1-selective inhibition with the antibody. We conclude that VCAM-1 is a promising biomarker candidate for monitoring BACE2 inhibition.

EXPERIMENTAL PROCEDURES

Animal Experiments

Female 2-3-year-old cynomolgus monkeys (*Macaca fascicularis*), which had not received any drug treatment before, were randomly divided into four groups of N = 4 animals each. Each group underwent treatment with one of the following compounds: a non-targeting control IgG, anti-RSV^{DC0018} (25) (referred to as IgG RSV), anti-BACE1^{DC0016} (25) (anti-BACE1), the blood–brain barrier penetrating construct ATV35.21.16:BACE1^{DC0181} (25) (ATV:BACE1), or verubecestat (26). IgG RSV, anti-BACE1, and ATV:BACE1 were intravenously administered once at a dose of 30 mg/kg. Verubecestat was administered at 10 mg/kg per dose (26) orally *via* nasogastric intubation. To achieve maximum Aβ reduction in the brain, verubecestat was applied twice with an interdose interval of 24 h.

Animals were sacrificed ~3 h after the second dose. In the other treatment groups, individuals were sacrificed 48 h after drug administration. Pre-dose CSF was taken twice at 20 and 10 h prior to treatment, respectively. Post-dose CSF was drawn directly before the animals were sacrificed. Pre-dose blood was sampled 10 h before treatment started. From the verubecestat-treated animals, post-dose blood was taken 2, 4, 8, 12, and 24 h after administration of the first dose as well as before termination. From the other treatment groups, blood was drawn directly after drug administration, 6 and 24 h thereafter, as well as prior to termination.

All animal experiments were conducted in agreement with ethical regulations and protocols approved by the Denali Therapeutics Institutional Animal Care and Use Committee. An overview of dosing and sampling time points for all treatment groups is provided in Supplemental Table S1.

CSF Withdrawal

Cynomolgus monkeys were intramuscularly injected with 0.04 mg/kg dexmedetomidine hydrochloride, followed by an intramuscular injection of 2.5 mg/kg ketamine hydrochloride ~10 min later to induce sedation. Animals were intubated, and ~1 ml of pre-dose CSF was collected *via* cisterna magna tap. Afterward, animals received an intramuscular injection of 0.2 mg/kg atipamezole hydrochloride to antagonize the sedation. Post-dose CSF was sampled directly before the monkeys were sacrificed by perfusion to obtain brain tissue. Animals were pre-sedated with dexmedetomidine hydrochloride as described earlier and received an intramuscular injection of 8 mg/kg ketamine hydrochloride 10 min later. Anesthetized animals were intubated and maintained on a mixture of isoflurane and oxygen, and 200 IU/kg heparin sodium was administered intravenously. A volume of ~1 ml CSF was collected *via* cisterna magna tap. Subsequently, monkeys were perfused with refrigerated 0.001% sodium nitrite in PBS *via* the left cardiac ventricle until complete blood removal.

Prior to pelleting potentially present red blood cells for 10 min at 2000*g* and 4 °C, a small CSF aliquot was removed and freeze-thawed to lyse any present red blood cells. Aliquots were then tested for hemoglobin *via* absorbance measurement at 280 nm and 417 nm. No blood contamination was detectable in any of the CSF samples.

Blood Withdrawal and Preparation of Plasma

At each of the time points indicated above, a volume of ~0.5 ml of peripheral venous blood was drawn using a needle and syringe and was collected in K2 EDTA blood collection tubes. Tubes were kept on ice for a maximum of 1 h until centrifugation at ~2000*g* and 4 °C for 15 min. The plasma was then split into two aliquots of approximately equal volumes and transferred to 0.75 ml Matrix storage tubes (Thermo Scientific). Samples were frozen on dry ice and stored at ≤ −60 °C.

Quantification of sAPPα, sAPPβ, and Aβ$_{40}$

sAPPα and sAPPβ in NHP CSF as well as Aβ$_{40}$ in CSF and plasma were quantified by ELISA as described previously (25).

Verubecestat Phase 1 Clinical Trial Samples

Human CSF was derived from a single ascending dose phase 1 study of verubecestat in healthy non-elderly volunteers. The human clinical study was conducted in accordance with International Conference on Harmonisation Good Clinical Practice guidelines and was approved by the relevant institutional review boards (P06498). The human CSF analysis abides the Declaration of Helsinki principles.

Each participant provided written informed consent. The full details of the study and study protocol were previously published (26). Participants were either dosed with placebo (N = 6) or 550 mg verubecestat (N = 5), and CSF was sampled 2 h before (pre-dose) and 24 h after treatment (post-dose).

CSF Preparation for Proteomic Analysis

For NHP CSF proteomics, single-pot, solid-phase-enhanced sample preparation (SP3) (30) was applied. 15 µl CSF was transferred to 1.5 ml tubes with low protein binding properties (Eppendorf or Thermo Scientific) and reduced with dithiothreitol (DTT, Biozol, 25 mM final concentration, 37 °C), followed by cysteine alkylation with iodoacetamide (IAA, Sigma-Aldrich, 80 mM final concentration, 24 °C, dark). The reaction was then quenched by adding another 2.5 µl of 200 mM DTT. A 1:1 mixture of hydrophobic and hydrophilic Sera-Mag SpeedBeads Carboxyl Magnetic Beads (Cytiva) with a final bead concentration of 4 µg/µl was prepared in water and 10 µl bead suspension was added to each sample. Proteins were bound to the beads by adding acetonitrile (Biosolve) to a final concentration of 70% (v/v) and shaking at 1000 rpm for 20 min. Beads were washed four times with 80% (v/v) ethanol (Sigma-Aldrich) using a magnetic rack (DynaMag-2, Thermo Fisher Scientific). Digestion was performed by adding 10 µl of 0.03 µg/µl LysC (Promega) in 50 mM ammonium bicarbonate (ABC) and incubating for 30 min at 37 °C and 1000 rpm, followed by 10 µl of 0.03 µg/µl trypsin (Promega) in 50 mM ABC and incubation for 16 h at room temperature. The supernatants were collected. A volume of 20 µl 0.1% formic acid (FA, Sigma-Aldrich) was added and combined with the supernatants, followed by filtration with 0.2 µm Costar Spin-X centrifuge filter tubes (Corning) to remove remaining beads. Samples were dried by vacuum centrifugation and dissolved in 20 µl 0.1% FA prior to liquid chromatography-coupled tandem mass spectrometry (LC-MS/MS) analysis.

Samples were prepared in four batches. To control for possible batch effects, pre-dose and post-dose samples from the same individual and one individual of each treatment group were processed in one batch.

Liquid Chromatography-Coupled Tandem Mass Spectrometry (LC-MS/MS)

To further minimize the risk of any systematic distortions of the analysis, preparation batches were measured in the sequence 1, 4, 2, and 3, with samples being placed in randomized order within each batch. Proteomic analyses were conducted on an EASY-nLC 1200 nanoUHPLC system (Thermo Fisher Scientific), coupled online to a Q Exactive HF Hybrid Quadrupol-Orbitrap mass spectrometer (Thermo Fisher Scientific) *via* a NanoFlex ion source that is equipped with a column oven (Sonation). A sample volume of 9 µl was added to 1 µl 2xiRT peptide standard (Biognosys), 10-fold diluted in 0.1% FA. A volume of 4.5 µl was injected into the LC-MS/MS system. Peptides were separated on a self-packed 30 cm C18 column (75 µm ID) with 1.9 µm ReproSil-Pur 120 C18-AQ resin (Dr. Maisch GmbH), using a binary gradient of 0.1% FA in water (A) and 0.1% FA in 80% acetonitrile (B) with a duration of 138.5 min and a flow rate of 250 nl/min. The gradient steps were as follows: 3% B at 0 min, 6% B at 2 min, 30% B at 92 min, 44% B at 112 min, 75% B at 121 min, 99% B at 123.5 min and until the end of the gradient. The column temperature was 50 °C.

Data-independent acquisition (DIA) was applied, including an MS1 full scan followed by 20 sequential DIA m/z windows for the generation of peptide fragment spectra (MS2). DIA windows had an overlap of 1 m/z and covered a total scan range of 300 to 1400 m/z. The width of the individual windows was as follows (indicated from first to last window): 85, 40, 30, 28, 26, 25, 24, 24, 24, 24, 25, 27, 28, 29, 34, 38, 46, 61, 151, 352 m/z. Positive ionization mode was applied. MS1 scans were acquired with a resolution of 120,000, an automatic gain control (AGC) target value of 5 x 10^6, and a maximum injection time of 120 ms. DIA windows were scanned with a resolution of 30,000 and an AGC target value of 3 x 10^6. The maximum injection time was chosen to be adjusted automatically in order to achieve optimal cycle times.

Proteomic Data Analysis

Processing of Raw Data—Mass spectrometric data were processed in DIA-NN (version 1.8) (31) using a library-free search. Trypsin (Trypsin/P) was defined as protease. Two missed tryptic cleavages and a maximum number of two variable modifications per peptide were allowed. Carbamidomethylation of cysteine residues was used as fixed modification, whereas N-terminal methionine excision, methionine oxidation, and protein N-terminal acetylation were considered as variable modifications. The precursor m/z range was adjusted to 300 to 1400 m/z, according to the DIA method settings. Match between runs was enabled. For all other parameters, default settings were used. Mass tolerances were automatically adjusted. Proteins were identified based on a *M. fascicularis* RefSeq FASTA database (downloaded on 16–03–2017, number of entries: 62,814). Protein and peptide false discovery rate (FDR) were set to 1%. A protein group was considered detected in a given sample when it was found with at least 2 peptides. NCBI GI numbers were translated into UniProt accession numbers *via* programmatic access of the UniProt ID mapping API (https://www.uniprot.org/help/id_mapping) with Python 3.9 using pandas 1.1.5–1.3.1, numpy 1.25.2 and requests 2.28.1.

Pearson Correlation—For quality control, samples were compared pairwise, and Pearson correlation coefficients (R) were calculated for the $\log_2$-transformed label-free quantification (LFQ) intensities of all protein groups that were detected (with at least 2 peptides) in both samples per comparison. To reduce matrix complexity, pre-dose samples of the same animal were first combined by calculating mean LFQ intensities. If a protein group was only detected in one of the pre-dose samples, the LFQ value of that sample was used instead of the mean. Correlation coefficients of >0.95 within samples were considered indicative of good technical reproducibility.

Pearson correlation coefficients were calculated and visualized in Python 3.9 using pandas 1.1.5, numpy 1.25.2, seaborn 0.12.2, and matplotlib 3.7.2.

Subcellular Location Analysis—Protein groups detected (with at least 2 peptides) in a minimum of 3 replicates per condition were grouped by their subcellular location as annotated in UniProt (32). Pre-dose samples of the same animal were combined by calculating mean LFQ intensities. If a protein group was only detected in one of the pre-dose samples, the LFQ value of that sample was used instead of the mean. Because of a low coverage of the UniProt database for *M. fascicularis*, the human proteome was used instead, restricted to all reviewed proteins. The database was downloaded in May 2024, considering both UniProt and Gene Ontology annotations, and was converted into one-hot-encoded format for the following annotation terms: cytoplasm, nucleus, endoplasmic reticulum, Golgi apparatus, mitochondrion, plasma membrane, GPI anchor, cell surface, extracellular space, plasma membrane external side, and secreted. Spelling or expression variants of those terms were included as well. In an additional (one-hot-encoded) category, each protein was either classified as a transmembrane protein or as not membrane-spanning.

UniProt database retrieval, database matching with sample data and visualization of the results were performed in Python 3.9 using pandas 1.1.5, numpy 1.25.2, requests 2.28.1, seaborn 0.12.2, and matplotlib 3.7.2. UniProt was programmatically accessed *via* its REST API (https://rest.uniprot.org/uniprotkb/search), and the following search categories (return fields; see also https://www.uniprot.org/

help/return_fields) were chosen: cc_subcellular_location, go_c, ft_transmem.

Comparison of the CSF Proteome Between the Treatment Groups—For each animal and protein group, LFQ intensities of the two pre-dose samples were averaged, followed by calculation of the post-dose/pre-dose ratio. If a protein group was only detected in one of the pre-dose samples, the LFQ value of that sample was used instead of the mean. A volcano plot was generated for each comparison between two treatments by plotting $\log_2$ fold changes of the post-dose/pre-dose ratios against negative $\log_{10}$ *p*-values obtained from an unpaired, two-tailed Student's *t* test. Volcano plots show all protein groups for which post-dose/pre-dose ratios could be calculated for at least 3 animals in each of the two treatment groups. From $\log_2$ transformation on, all calculations and generation of the plots were conducted in Python 3.9 by the help of pandas 1.1.5–1.3.1, numpy 1.25.2, scipy 1.11.2, seaborn 0.12.2, and matplotlib 3.7.2. FDR threshold curves were calculated in Perseus (version 1.6.10.45) (33) based on 250 random permutations, a significance threshold of 0.05 and s0 = 0.1, and were imported into Python for plotting.

In addition, post-dose/pre-dose ratios of selected BACE substrates or substrate candidates, respectively, were visualized on linear scale in GraphPad Prism (versions 9.5.1–10.2.2) (GraphPad Software).

Peptide Localization Mapping—To test whether identified peptides of selected BACE substrates or substrate candidates, respectively, arose from the extracellular domain, peptide sequences were aligned with the entire protein sequence and their localization visualized on a domain-annotated graphical representation of the protein. Only unique peptides were plotted. Information on protein sequences and domains was retrieved from UniProt (32) *via* programmatic access to the UniProt REST API (https://rest.uniprot.org/uniprotkb/search) using the following return fields (see also https://www.uniprot.org/help/return_fields): sequence, length, ft_signal, ft_topo_dom, ft_transmem, ft_intramem, ft_propep. When UniProt domain annotations did not cover the whole protein sequence, the Phobius web server (https://phobius.sbc.su.se/) (34) was accessed *via* its REST API (https://www.ebi.ac.uk/Tools/services/rest/phobius), and protein domain information was inferred from Phobius predictions instead. If a protein's GI number could not be translated into a UniProt accession number, the UniProt accession number of the longest available isoform was chosen. In case not all peptides matched with one and the same isoform, the analysis was performed for all available isoforms. If a protein was not found in UniProt, or if not all peptides of a protein matched with the UniProt sequence, the RefSeq database in combination with Phobius was used instead. Peptide localization mapping was done in Python 3.9 using pandas 1.1.5–1.3.1, numpy 1.25.2, requests 2.28.1, seaborn 0.12.2, and matplotlib 3.7.2. The whole analytic approach was inspired by the QARIP web server (https://webclu.bio.wzw.tum.de/qarip/) (35).

VCAM-1 Detection by Western Blotting

A volume of 15 µl NHP or human CSF was mixed with 5 µl of 4x Laemmli buffer that contained 400 mM DTT (instead of β-mercaptoethanol), and samples were incubated at 95 °C for 5 min. After cooling down at room temperature and brief centrifugation, samples were separated on 8% SDS-polyacrylamide gels until the 50 kDa marker band almost reached the bottom of the gel. Proteins were transferred onto nitrocellulose membranes using the Trans-Blot Turbo RTA Transfer Kit, Nitrocellulose in combination with the Trans-Blot Turbo Transfer System (Bio-Rad). Albumin served as a loading control and was detected with help of the MemCode Reversible Protein Stain Kit for nitrocellulose membrane (Thermo Scientific), following the manufacturer's instructions for staining and de-staining. Afterward, membranes were blocked for 30 min at room temperature in Blocker FL Fluorescent Blocking Buffer (10x) (Thermo Scientific), 10-fold diluted in water. Blocked membranes were rinsed three times with PBST (phosphate-buffered saline with 0.05% Tween 20) and incubated with anti-VCAM-1 primary antibody (AF809, R&D Systems), diluted 1:250 in PBST with 0.25% BSA and 0.025% NaN_3, for 2 to 3 days at 4 °C. After washing three times in PBST for 5 min, either an HRP-conjugated (A16050, Thermo Scientific) or a fluorophore-coupled (Alexa Fluor 680, A-21102, Invitrogen) anti-sheep secondary antibody was added for 1 to 2 h at room temperature, diluted 1:5000 in PBST with 0.25% BSA (HRP-conjugated), or diluted in the 1x blocking buffer (fluorophore-coupled antibody). Membranes were washed another three times in PBST, and VCAM-1 was detected either using ECL Prime (Amersham) with an incubation time of 5 min or by fluorescence imaging, respectively.

Alternatively, a volume of 9 or 10 µl CSF was mixed with 3 or 4 µl, respectively, of the Laemmli buffer, and proteins were separated on 10% Mini-Protean TGX Precast Protein Gels (Bio-Rad).

Albumin and VCAM-1 signal intensity was quantified in ImageJ (version 1.52a, National Institute of Health, USA). Signal intensities within equally sized rectangles, drawn around each band, were displayed as intensity curves, and peak bottom lines were defined individually for the respective intensity peaks. Subsequently, the area under the curve was quantified, and, for each lane, the VCAM-1 signal area was normalized to that for albumin.

Identification of Semi-Specific VCAM-1 Peptides in CSF

Sample Preparation—To identify the BACE2 cleavage site within VCAM-1, NHP CSF before and after treatment with verubecestat was digested with GluC and analyzed *via* a modified version of TermineR (36) for the identification of peptides arising from endogenous proteolytic cleavage. Equal volumes of the two pre-dose samples per animal were pooled, resulting in one pre-dose and one post-dose sample per animal. 12 µl of each CSF sample were transferred onto a 96-well plate, and samples were processed by a modified, automated version of the SP3 protocol above. 20 µl STET buffer with 2% Triton X-100 were added per well, followed by 2.5 µl 200 mM DTT and protein reduction for 30 min at 45 °C. Samples were then alkylated with 5 µl 400 mM chloroacetamide for 30 min at 25 °C. Wells were provided with 5 µl of the SP3 bead suspension and ethanol to a final concentration of 80% (v/v). After protein binding and washing of the beads, 35 µl of 0.5 µg GluC (Promega) in 50 mM ABC pH 8.0 were added per well and the plate was incubated at 37 °C overnight. After a short spinning of the plate, it was briefly shaken and put onto the magnetic place holder for 5 min to adhere the beads. Samples were then filtered and dried as described above and were resuspended in 18 µl 0.1% FA.

LC-MS/MS—A sample volume of 4 µl was analyzed on a TimsTOF Pro mass spectrometer (Bruker) equipped with a CaptiveSpray ion source and coupled online to a nanoElute HPLC system (Bruker). Peptides were separated on a 15-cm self-packed C18 column (75 µm ID, 1.9 µm C18 resin particles) at 50 °C applying a binary gradient of 0.1% FA in water (A) and 0.1% FA in acetonitrile (B) with the following steps: 2% B at 0 min, 24% B at 62 min, 35% B at 72 min, 85% B at 77 min. A flow rate of 300 nl/min was applied.

DIA was combined with parallel accumulation-serial fragmentation (PASEF) and trapped ion mobility spectrometry (TIMS) with a ramp time of 100 ms. One MS1 full scan was followed by 26 sequential MS2 DIA m/z windows, each having a width of 27 m/z. A total scan range of 350 to 1002 m/z was covered with a cycle time of 1.4 s and in positive ionization mode.

For spectral library generation, samples were additionally analyzed with data-dependent acquisition (DDA). The 10 most intense precursor ions were selected for fragmentation. Dynamic exclusion was used to avoid overrepresentation of the highest abundant precursor ions. One DDA-PASEF MS1 scan was followed by 10 MS2 scans with a total

cycle time of 1.1 s and an m/z range of 100 to 1700. The ion mobility range was 0.6 to 1.45 Vs/cm^2. Precursor ion fragmentation was achieved by collision-induced dissociation (CID) at an energy range of 20 to 59 eV and with a width of 2 m/z.

Analysis of Raw Data—Data were processed in Fragpipe (version 22.0) (37) applying the DIA-SpeclibQuant workflow including DIA as well as DDA data for spectral library generation. Standard settings were used for diaPASEF spectrum deconvolution (version 1.1.5) and MSFragger (version 4.1) except for the following modifications: Search parameters were adjusted to the detection of semi-specific peptides cleaved by GluC, while potential cleavage C-terminally of aspartate was ignored. The precursor mass tolerance was set to 20 ppm and the allowed peptide length to 5 to 50 amino acids. One missed cleavage and a maximum number of 5 variable modifications were allowed. Protein N-terminal methionine excision or oxidation as well as N-terminal acetylation were considered as variable modifications. Cysteine carbamidomethylation was included as fixed modification. Samples were analyzed with the same *M. fascicularis* FASTA database as described above. Protein and peptide quantification was performed in DIA-NN (version 1.8.2).

To validate the outcome of TermineR, which is still a relatively new approach and not yet widely established, data were additionally analyzed in Spectronaut (version 18.3, Biognosis), using the directDIA workflow that was adapted as described earlier. Two missed GluC cleavages were allowed. As in Fragpipe, DDA measurements were included for spectral library generation.

VCAM-1 Peptide Localization Mapping and Quantitative Analysis—Duplicate peptides (*e.g.* due to detection at different charge states) were summarized by summation of LFQ intensity values. For each animal, post-dose LFQ values of VCAM-1 peptides were then normalized to the respective pre-dose values. Peptide localization within the VCAM-1 sequence was analyzed as described above, including peptide color coding for the individual $\log_2$-transformed post-dose/pre-dose ratios as well as the indication of unspecific termini resulting from endogenous proteolytic cleavage.

Comparison With Data From Tryptic Digestion—To compare protein LFQ intensity values from GluC digestion with the trypsin dataset, volcano plots were generated for both the Fragpipe and the Spectronaut data. Volcano plots were computed as described above, including all protein groups that were detected in at least 3 samples in each group, for the comparison of $\log_2$ fold changes of post-dose *versus* pre-dose intensity values.

Besides, post-dose LFQ values were normalized to the corresponding pre-dose values, and post-dose/pre-dose ratios for selected BACE substrates or substrate candidates, respectively, were plotted on linear scale as described earlier.

BACE2 Cleavage Assay of VCAM-1

Sample Preparation—A synthetic *M. fascicularis* VCAM-1 peptide with the sequence KVGSQLRSLTLDVQGRENNK, which spans the potential BACE2 cleavage site and is identical with the respective region in human VCAM-1, was ordered from JPT. The peptide was dissolved in 50 mM sodium acetate pH 4.4, and 0.5 μg of the peptide were incubated with 0.5 μg recombinant human BACE2 (R&D Systems) overnight at 37 °C. The reaction was performed in 50 mM sodium acetate buffer pH 4.4 in a total volume of 20 μl. In parallel, the synthetic peptide was incubated without BACE2 or with BACE2 together with 10 μM verubecestat (Sigma-Aldrich). Peptides were then purified for mass spectrometry using C18 STAGE Tips (38).

LC-MS/MS—2.5 ng of peptide input were analyzed on an Orbitrap Exploris 480 mass spectrometer (Thermo Scientific) in combination with a Vanquish Neo UHPLC system (Thermo Scientific). Samples were loaded with trap-and-elute injection. A PepSep 15 cm × 75 μm column with 1.9 μm C18 resin particles (Bruker), linked to a 10 μm PepSep Emitter FS with liquid junction (Bruker), was used for peptide separation at a column temperature of 40 °C. Separation was achieved using a binary gradient with 0.1% FA in water (A) and 0.1% FA in 80% (v/v) acetonitrile (B) at a flow rate of 300 nl/min. The gradient composition was as follows: 6% B at 0 to 1 min, 31% B at 25 min, 50% B at 27 min, 95% B at 29 to 37 min, and 6% B at 39 min.

Peptides were analyzed in DDA mode with one MS1 scan followed by 20 MS2 scans at a resolution of 120,000 and 15,000, respectively. The total scan range was 300 to 1400 m/z and the precursor isolation window 1.6 m/z. Precursor ions with a charge state of 2 to 6 were considered. Dynamic exclusion was used with an exclusion time of 4 s. Positive ionization was applied and peptides were ionized with a Nanospray Flex Ion Source (Thermo Scientific). A normalized AGC target of 300% (MS1) and 100% (MS2) was used. RF lens was set to 45%. Fragments were generated by higher energy collisional dissociation (HCD) at a normalized energy level of 28%.

Analysis of Raw Data—Data were analyzed in Fragpipe using a self-written FASTA file exclusively including human VCAM-1. The LFQ-MBR workflow was applied with the following adjustments: Normalization across runs and match between runs were omitted and an unspecific search was conducted with a protein FDR filter of 1. N-terminal methionine excision and methionine oxidation were included as modifications. A minimum peptide length of 6 amino acid was allowed. Total ion chromatograms were obtained with Xcalibur (version 4.5.47.0, Thermo Scientific). The Fragpipe-PDV viewer was used to extract and export annotated MS2 spectra. Total ion chromatograms were plotted in GraphPad Prism (version 10.2.1).

Statistics

Statistical analyses were performed in Python 3.9, Perseus (version 1.6.10.45) and GraphPad Prism (versions 9.5.1–10.4.0). Details are stated in the figure legends and in the method sections above.

Experimental Design and Statistical Rationale

We treated cynomolgus monkeys either with the selectively BACE1 inhibiting construct ATV:BACE1 or the unselective, BACE1 and BACE2 inhibiting compound verubecestat and compared the CSF proteomes in a label-free quantitative LC-MS/MS approach using DIA. Treatment with the non-targeting antibody IgG RSV or a non-brain-penetrating anti-BACE1 antibody served as controls (N = 4 in each group). To account for inter-individual variability, post-dose/pre-dose ratios for the identified protein groups were calculated for each animal prior to the comparison between the treatment groups. Protein groups with a Student's *t* test *p*-value below 0.05 were considered significantly changed in abundance. VCAM-1 was identified as the only protein being shed by BACE2 but not BACE1. Results for VCAM-1 were validated by western blotting. Soluble VCAM-1 (sVCAM-1) levels were further shown to also decrease in human CSF in response to verubecestat. To identify the BACE2 cleavage site of VCAM-1, we re-analyzed the NHP CSF samples of the verubecestat group using GluC for digestion and applying semi-specific cleavage specificity for the data analysis. The identified cleavage site was validated by an *in vitro* cleavage assay with a synthetic VCAM-1 peptide and recombinant BACE2.

RESULTS

Reduction of CSF Aβ upon BACE1 Inhibition

To identify a CSF biomarker that reflects BACE2 activity in the brain, we analyzed the CSF proteome of NHPs (*M. fascicularis*) treated with either an antibody specifically targeting BACE1 (25) or with the clinically tested small-

molecule drug verubecestat, which blocks both BACE1 and BACE2 (26) (Fig. 1*A*). To enhance antibody uptake into the brain, the BACE1 antibody was modified to carry a binding sequence for the transferrin receptor, referred to as antibody transport vehicle (ATV:BACE1) (25). As a control, the same antibody but without the ATV sequence was used (anti-BACE1). This antibody does not efficiently cross the blood–brain barrier and does not lower CSF Aβ levels (25). As a further control, an IgG antibody was used that does not target any NHP protein (IgG RSV).

CSF was sampled from two time points prior to dosing (–10 h and –20 h) and served as baseline for the proteomic measurements. CSF was also collected at 48 h after a single dose of the three IgGs and at ~3 h after the last of two doses

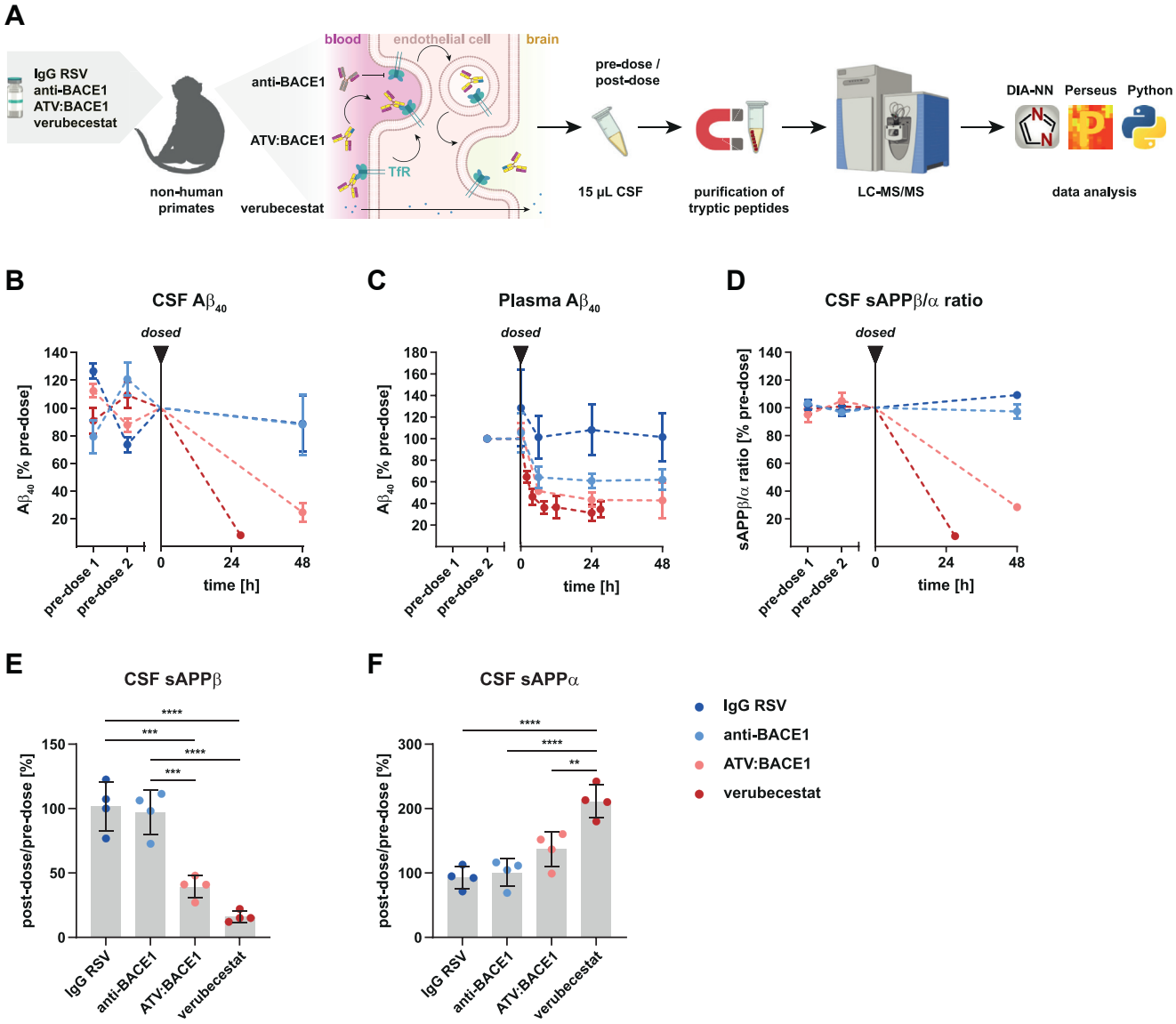

FIG. 1. **ATV:BACE1 and verubecestat reduce $A\beta_{40}$ levels and the sAPPβ/α ratio in NHP plasma and CSF.** *A*, NHP CSF proteomics workflow. NHPs were treated with 30 mg/kg of IgG RSV, anti-BACE1, ATV:BACE1, which is able to cross the blood-brain barrier *via* the transferrin receptor (TfR), or two 10 mg/kg doses (24 h apart) of verubecestat. Animals were taken down 48 h after dosing for the antibodies and 2 to 6 h after the last dose of verubecestat. The total CSF proteome was digested and purified and analyzed by liquid-chromatography-coupled tandem mass spectrometry using data-independent acquisition (DIA). Data analysis was performed in DIA-NN, Perseus and Python. The figure was created with BioRender.com. $A\beta_{40}$ determined in (*B*) CSF and (*C*) plasma from NHPs either treated with IgG RSV, anti-BACE1, ATV:BACE1 or verubecestat (N = 4 in each group). Values are normalized to the mean of two pre-dose samples, taken 20 h (pre-dose 1) and 10 h (pre-dose 2) before treatment start (dosed). Pre-dose means are set to 100% and mark the treatment starting point (dosed). *D*, the sAPPβ/α ratio in CSF from the same experiment. *E*, sAPPβ and (*F*) sAPPα concentrations are displayed separately. One-way ANOVA followed by Tukey's multiple comparisons test. Only significant differences are indicated. $^{**}p < 0.01$, $^{***}p < 0.001$, $^{****}p < 0.0001$. All data depict mean and SD.

of verubecestat, with an inter-dose interval of 24 h. Time points were chosen based on previous data on maximum Aβ reduction in NHPs for ATV:BACE1 (25) and verubecestat (26). Target engagement was monitored measuring changes of $Aβ_{40}$ concentrations in CSF and plasma (Fig. 1, *B* and *C* and Supplementary Fig. S1*A*). Additionally to Aβ, two other APP cleavage products were measured: the BACE1 cleavage product sAPPβ and the α-secretase cleavage product sAPPα. Both ATV:BACE1 and verubecestat strongly reduced the $Aβ_{40}$ concentration in both CSF and plasma as well as CSF sAPPβ at the time points examined (Fig. 1, *D* and *E*). The effect size for verubecestat was stronger than for ATV:BACE1, as seen for example with the degree of CSF $Aβ_{40}$ reduction of more than 90% for verubecestat versus 75% for ATV:BACE1. As expected, the control treatment with IgG RSV did not alter the concentration of the APP cleavage products, while the anti-BACE1 antibody without the brain-targeting ATV sequence only reduced $Aβ_{40}$ in plasma, but not in CSF (Fig. 1, *B–E* and Supplemental Fig. S1).

Since BACE1 and "a disintegrin and metalloproteinase" 10 (ADAM10), the main α-secretase (5), compete for APP as a substrate, inhibition of BACE1 is concomitant with increased APP α-cleavage, resulting in elevated amounts of sAPPα (39). This was also seen for verubecestat (Fig. 1*F*), in agreement with results from a clinical trial with that compound (26). As a result, the ratio of the concentrations of sAPPβ and sAPPα was strongly reduced for verubecestat with a higher effect size than for treatment with ATV:BACE1 and similar to the $Aβ_{40}$ reduction (Fig. 1*D* and Supplemental Fig. S1*B*). Therefore, we conclude that verubecestat, similar to ATV:BACE1, shows excellent target engagement on BACE1 in the brain.

Change in NHP CSF Proteome After Inhibition of BACE1 and BACE2

To identify changes beyond APP processing in the NHP CSF proteome induced upon inhibition of BACE1 and BACE2, we subjected pre-dose and post-dose CSF samples to proteomic analysis (workflow in Fig. 1*A*). We identified 2130 protein groups in total that were detected with at least two peptides. The excellent technical reproducibility of the analysis and the good sample quality are reflected by high Pearson correlation coefficients for the overall protein intensities among the different samples, mostly exceeding 0.96 for samples from the same donor NHP and above 0.9 for the majority of all other comparisons (Supplemental Fig. S2*A*). As a further quality control, we used the subcellular location annotations of the identified proteins, which showed that mainly secreted and plasma membrane proteins (potentially released by proteolytic cleavage) as well as proteins located in the extracellular space were detected (Supplemental Fig. S2*B*). In contrast, mitochondrial proteins, an indicator of potential cellular contamination, belonged to the three least abundant groups (Supplemental Fig. S2*B*).

Next, we performed a relative label-free protein quantification to identify abundance changes between the groups. Compared to the IgG RSV control, treatment with the non-brain-targeting anti-BACE1 antibody did not induce significant changes in the overall NHP CSF proteome after FDR correction (Fig. 2*A*). The lack of BACE inhibition in the CSF was also seen for 12 BACE substrates or substrate candidates (18, 28, 29, 40–44) (Table 1).

Tryptic peptides identified from those BACE substrates mapped exclusively to the ectodomain and not the transmembrane or cytoplasmic domain, therefore representing shed ectodomains and not full-length transmembrane or GPI-anchored proteins being released from brain into CSF (Fig. 2*B*).

Compared to the IgG RSV control, ATV:BACE1 and verubecestat induced very specific changes in the CSF proteome, as seen with the reduced CSF abundance of the BACE1 cleavage products of several of the BACE substrates highlighted in Figure 2*A*, including interleukin-6 receptor subunit β (IL6ST, gp130) and "VWFA and cache domain-containing protein 1" (CACHD1), which showed both the strongest treatment-mediated response, reaching a reduction of up to 75% for verubecestat compared to IgG RSV control (Fig. 2*A*). Clear reductions were also seen for most other BACE substrates and substrate candidates, including amyloid β precursor like protein 1 (APLP1), basigin (BSG), contactin-2 (CNTN2), leucine-rich repeat neuronal protein 1 (LRRN1), seizure protein 6 homolog (SEZ6), and seizure 6-like protein (SEZ6L) (Figs. 2*A* and 3). In line with the results on Aβ (Fig. 1*B* and Supplemental Fig. S1*A*), verubecestat appeared to reduce the abundance of BACE1 substrates in CSF slightly stronger than ATV:BACE1. Most of the changes for verubecestat reached statistical significance, even after FDR correction for multiple testing. The protein changes seen for ATV:BACE1 trended similarly but were less robust compared to verubecestat (Fig. 3), and did not all reach significance, given the slightly higher variability among the ATV:BACE1 samples compared to the verubecestat samples (Supplemental Fig. S2*A*).

Identification of VCAM-1 as a CSF Protein Marker for BACE2 Activity

To identify a protein that may be changed in CSF in response to inhibition of BACE2 but not BACE1, we compared the proteomic CSF abundance changes between verubecestat (BACE1 and BACE2 inhibition) and the specific BACE1 inhibition by ATV:BACE1 (Figs. 2*A*, 3, and Table 1). VCAM-1 was the only protein that showed a significant reduction of more than 50% upon verubecestat treatment, while its CSF abundance was not altered in response to the selective inhibition of BACE1 with ATV:BACE1 (Figs. 2*A*, 3, and Supplemental Fig. S3). CACHD1 and LRRN1 also showed a stronger reduction in their cleaved ectodomains in CSF upon treatment with verubecestat compared to ATV:BACE1 (Fig. 3),

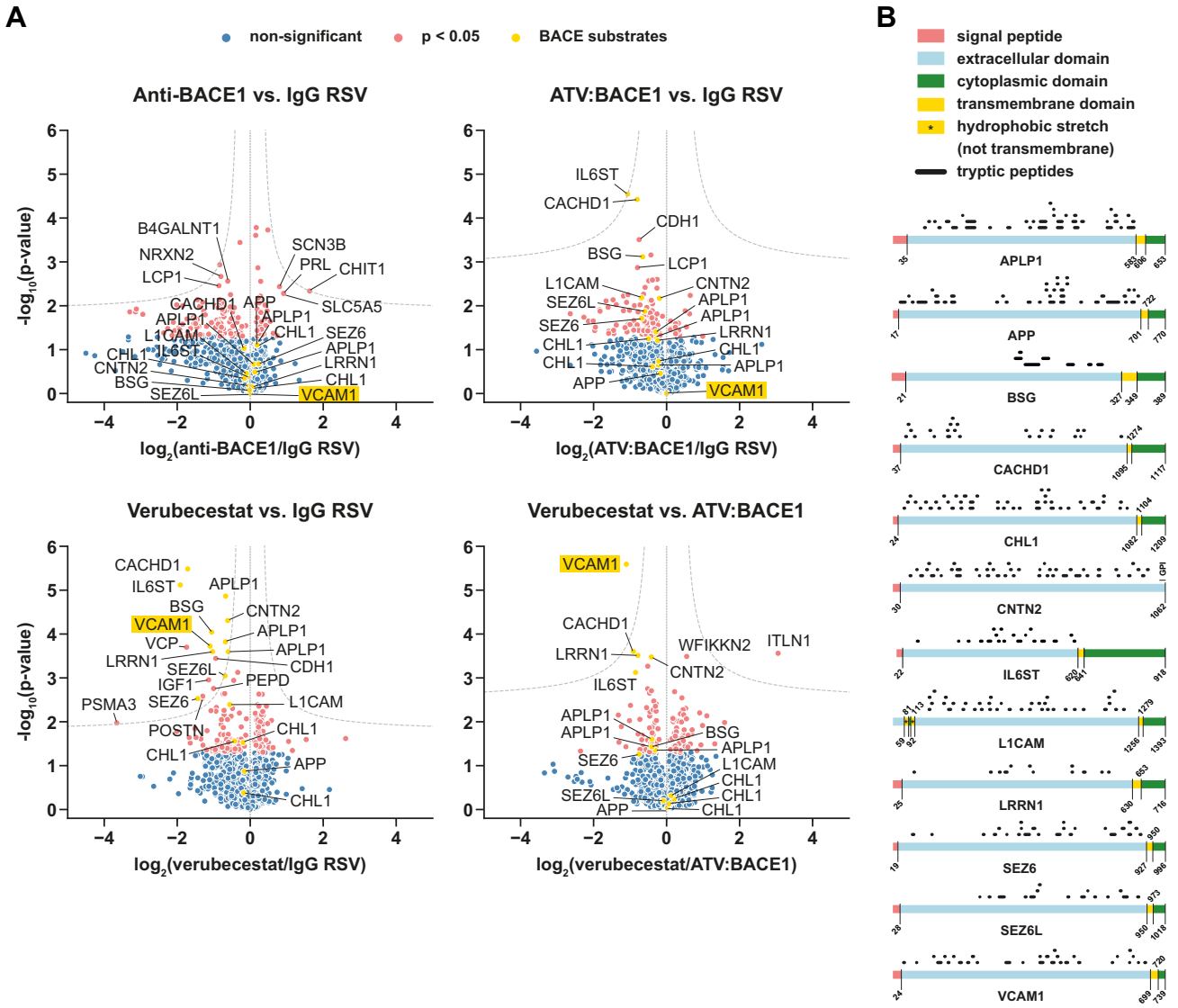

FIG. 2. **Verubecestat but not ATV:BACE1 treatment reduces VCAM-1 in NHP CSF.** *A*, volcano plots of the proteomic analysis of CSF from cynomolgus monkeys treated with anti-BACE1, ATV:BACE1 or verubecestat against CSF from IgG RSV-treated animals as control (N = 4 for all treatment groups). In addition, CSF proteomes for ATV:BACE1 and verubecestat treatment were compared directly with each other. For each animal and protein group, LFQ intensities of the two pre-dose samples were averaged, followed by calculation of the post-dose/pre-dose ratio. For each comparison, $\log_2$ fold changes of those ratios are plotted against negative $\log_{10}$ *p*-values obtained from an unpaired, two-tailed Student's *t* test. Dashed hyperbolic curves represent a permutation-based FDR significance threshold. Volcano plots show all protein groups for which post-dose/pre-dose ratios could be calculated for at least 3 (out of 4) animals in both of the compared treatment groups. Selected BACE substrates or substrate candidates are labeled with their gene names and highlighted in yellow. *B*, localization and length of the identified unique peptides for the BACE substrates or substrate candidates. Protein domains are depicted according to UniProt information in case of APP and based on Phobius predictions for all the other proteins. For APLP1 and CHL1, peptides from different isoforms were detected. In either case, the longest definitely detected isoform is displayed. Because IL6ST is currently not included in the UniProt *Macaca fascicularis* database, the RefSeq database was used instead. Likewise, peptides for BSG were mapped on the RefSeq database sequence (the longer of two isoforms), since not all peptides matched the UniProt sequence. Based on the sequence of human L1CAM, the N-terminal regions, which in Phobius were predicted to be transmembrane domains, most likely are not membrane-spanning and are therefore referred to as hydrophobic stretches.

but the difference between both conditions did not reach statistical significance and may be explained by the slightly stronger BACE1 inhibition by verubecestat compared to ATV:BACE1 that was also seen for the reduction of CSF Aβ (Fig. 1*B* and Supplemental Fig. S1*A*).

VCAM-1, which is also known as CD106, is a single-span transmembrane protein with a large extracellular domain containing seven Ig-like domains (Fig. 4*A*). VCAM-1 undergoes shedding at a peptide bond within the extracellular juxtamembrane domain, resulting in the release of the soluble VCAM-1

TABLE 1
Fold changes and p-values on linear scale for selected BACE substrates and substrate candidates

BACE substrate			Anti-BACE1 *versus* IgG RSV			ATV:BACE1 *versus* IgG RSV			Verubecestat *versus* IgG RSV			Verubecestat *versus* ATV:BACE1		
Gene name	NCBI GI number	UniProt ac	Fold change	*p*-value	FDR	Fold change	*p*-value	FDR	Fold change	*p*-value	FDR	Fold change	*p*-value	FDR
APLP1	544510679; 545687855	A0A2K5WNL8; Q4R4M8	1.13	7.38E-02	–	0.82	3.93E-02	–	0.66	2.53E-04	+	0.81	4.46E-02	–
APLP1	544510679	A0A2K5WNL8	1.07	2.14E-01	–	0.83	5.62E-02	–	0.63	1.51E-04	+	0.76	2.51E-02	–
APLP1	545687855	Q4R4M8	1.09	3.24E-01	–	0.86	2.24E-01	–	0.63	1.37E-05	+	0.73	3.67E-02	–
APP	544418429; 544418433	P53601	1.14	7.82E-02	–	0.89	3.49E-01	–	0.90	1.35E-01	–	1.01	9.45E-01	–
BSG	544507304; 544507306	G7PY34	0.98	8.44E-01	–	0.64	7.65E-04	–	0.48	9.04E-05	+	0.76	3.73E-02	–
CACHD1	544405449	A0A2K5WIQ0	0.89	9.35E-02	–	0.57	3.77E-05	–	0.31	3.28E-06	+	0.53	2.50E-04	–
CHL1	544415461; 544415463; 982235508	A0A2K5U5H2; A0A2K5U5M5	1.14	7.89E-02	–	0.86	1.84E-01	–	0.87	2.97E-02	–	1.01	8.91E-01	–
CHL1	544415461; 982235508	A0A2K5U5H2	1.04	7.19E-01	–	0.71	5.65E-02	–	0.74	2.75E-02	–	1.05	7.39E-01	–
CHL1	544415463	A0A2K5U5M5	0.89	4.50E-01	–	0.76	2.44E-01	–	0.88	4.18E-01	–	1.16	5.78E-01	–
CNTN2	544399713; 544399717; 982223057	A0A2K5WM05	0.98	6.87E-01	–	0.87	6.76E-03	–	0.65	4.92E-05	+	0.75	3.34E-04	–
IL6ST	544437205	-	0.95	4.19E-01	–	0.48	2.85E-05	–	0.26	7.61E-06	+	0.55	7.51E-04	–
L1CAM	544523692; 544523701; 544523704; 544523707; 544523710	A0A2K5UR40; A0A2K5UR71	0.93	3.48E-01	–	0.62	6.54E-03	–	0.68	4.06E-03	–	1.09	4.85E-01	–
LRRN1	544415526; 982235525	G7NYW8	1.03	7.08E-01	–	0.84	6.18E-02	–	0.49	2.51E-04	+	0.58	3.07E-04	–
SEZ6	544497964; 544497966; 982304437; 982304439; 982304443	A0A2K5WPJ4	1.18	2.11E-01	–	0.62	1.94E-02	–	0.37	2.96E-03	+	0.59	5.48E-02	–
SEZ6L	544462825; 544462827; 544462829; 982272701; 982272705	A0A2K5UD37	1.00	9.83E-01	–	0.66	1.34E-02	–	0.62	8.98E-04	–	0.94	6.34E-01	–
VCAM1	544404125	G7NV32	1.00	9.80E-01	–	1.00	9.90E-01	–	0.47	1.89E-04	+	0.47	2.57E-06	+

Linear fold changes and *p*-values are given for all BACE substrates and substrate candidates, respectively, that are highlighted in the volcano plots in Figure 2*A*. Significance after FDR correction is indicated with "+", whereas non-significant changes are indicated with "–". APLP1 and CHL1 were identified in three protein groups each, with every protein group representing a different isoform or combination of isoforms, as it is reflected by the corresponding GI and UniProt accession numbers. No UniProt accession number could be assigned to IL6ST, since this protein is currently not part of the UniProt *Macaca fascicularis* database.

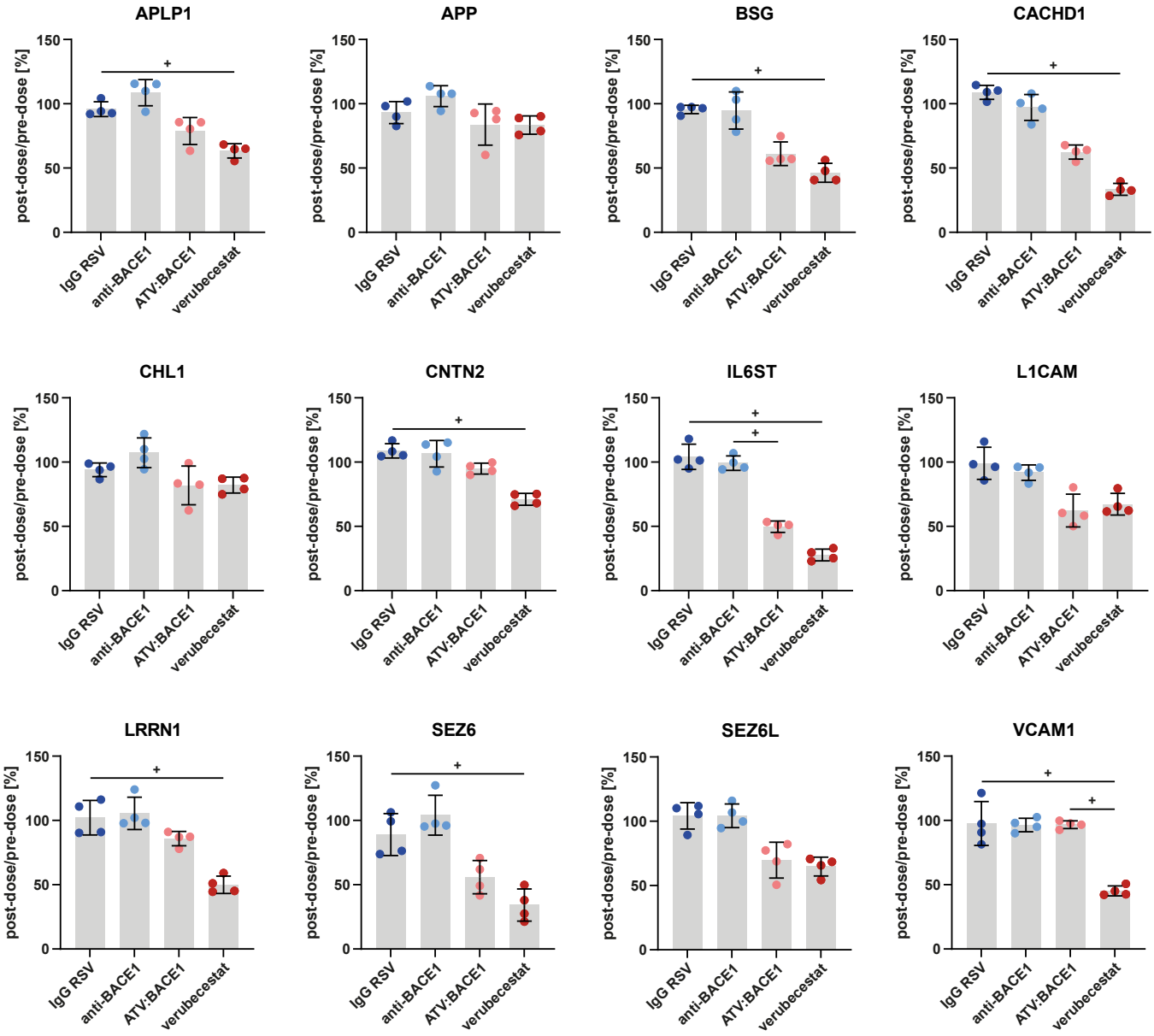

FIG. 3. **Post-dose to pre-dose ratios of BACE substrates and substrate candidates**. Dot plots of post-dose/pre-dose protein LFQ intensity ratios for selected BACE substrates or substrate candidates. CSF from cynomolgus monkeys treated with IgG RSV, anti-BACE1, ATV:BACE1 or verubecestat (N = 4 in each group) was proteomically analyzed, and ratios were calculated of post-dose intensities and the mean intensities of the two pre-dose samples. Plus signs indicate FDR significance in the volcano plot of the respective comparison (Fig. 2*A*). For APLP1 and CHL1, which were detected in three protein groups each, the protein group with the most identified peptides is displayed. All data depict mean and SD.

ectodomain (sVCAM-1) (Fig. 4*A*). Our proteomic measurements had revealed that the tryptic peptides identified for VCAM-1 in CSF specifically map to sVCAM-1 and not full-length VCAM-1, as they aligned with the extracellular, but not the transmembrane or cytoplasmic domain of VCAM-1 (Fig. 2*B*).

To validate the proteomic result of VCAM-1 being shed by BACE2 but not BACE1, we used immunoblotting as an orthogonal method and, upon verubecestat treatment, detected changes in sVCAM-1 levels in the same CSF samples of the four distinct NHPs. The reduction of sVCAM-1 in immunoblot analysis upon treatment with verubecestat was more than 50% (Fig. 4, *B* and *C*), while ATV:BACE1 did not alter sVCAM-1, which is in excellent agreement with the proteomic results (Figs. 2*A*, 3, and Table 1).

We conclude that sVCAM-1 in NHP CSF results from shedding by BACE2 but not BACE1, suggesting that sVCAM-

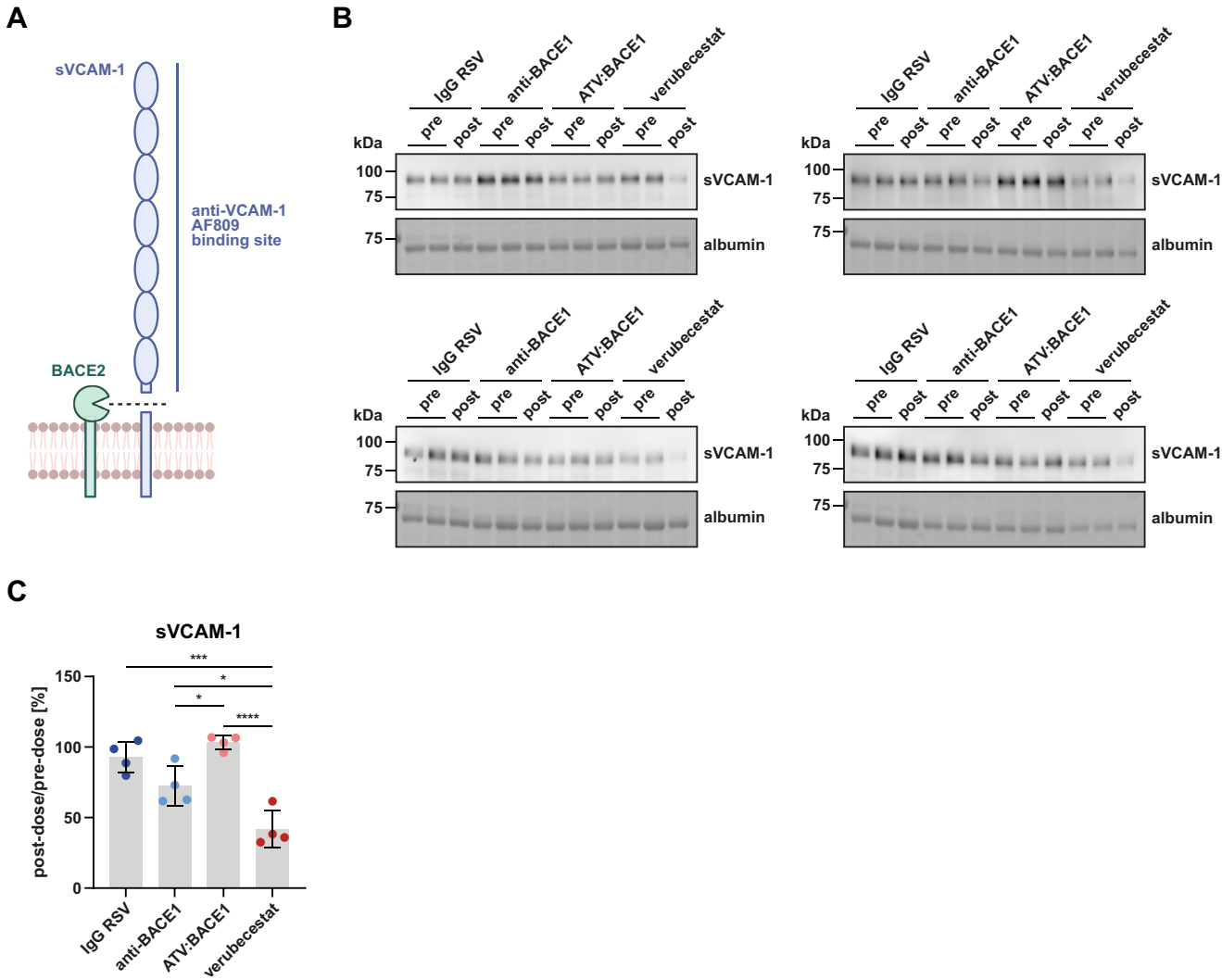

FIG. 4. **Western blot validation of VCAM-1 as BACE2 substrate.** *A*, scheme of VCAM-1 cleavage by BACE2. Mapping of detected peptides (Fig. 2*B*) suggests that VCAM-1 is shed closely above the plasma membrane. Western blotting was conducted with a polyclonal antibody that specifically targets the ectodomain. The figure was created with BioRender.com. *B*, Western blot detection of sVCAM-1 in CSF from cynomolgus monkeys treated with IgG RSV, anti-BACE1, ATV:BACE1 or verubecestat (N = 4 in each group). Albumin served as loading control and was visualized by total protein staining. *C*, quantification of Western blot results in *B*. First, sVCAM-1 signal intensities were normalized to albumin. For each individual, the two pre-dose values were averaged, followed by calculation of the post-dose/pre-dose ratio. Data depict mean and SD. One-way ANOVA in combination with Tukey's multiple comparisons test. Only significant differences are indicated. $^{*}p < 0.05$, $^{***}p < 0.001$, $^{****}p < 0.0001$.

1 may be useful as a marker to monitor changes in BACE2 activity in the brain.

Verubecestat Reduces sVCAM-1 Levels Also in Human CSF

To further investigate whether our results for sVCAM-1 in NHP CSF also apply to human CSF, we analyzed CSF samples from healthy non-elderly phase 1 clinical trial participants (26), who either received a single dose of 550 mg verubecestat or placebo, by immunoblotting (Fig. 5*A*). Samples were taken 2 h before and 24 h after dosing. In the placebo group, sVCAM-1 levels were found to be elevated by about 80% in the post-dose compared to the pre-dose samples (Fig. 5*B*). Similar effects were also apparent for sAPPβ, $A\beta_{40}$, and $A\beta_{42}$ levels, as measured previously in the same samples (26), with an increase of 57%, 53% and 68% in the post-dose relative to the pre-dose samples, respectively (Supplemental Fig. S4). Such an increase in AD-related biomarkers over time was also reported in other studies (*e.g.* (45–47)) and is considered as a consequence of frequently repeated CSF sampling (47, 48) as well as diurnal variability (46, 48, 49).

Within the verubecestat group, sVCAM-1 in the post-dose samples decreased by more than 40% when compared to pre-dose CSF and by about 70% in relation to the placebo

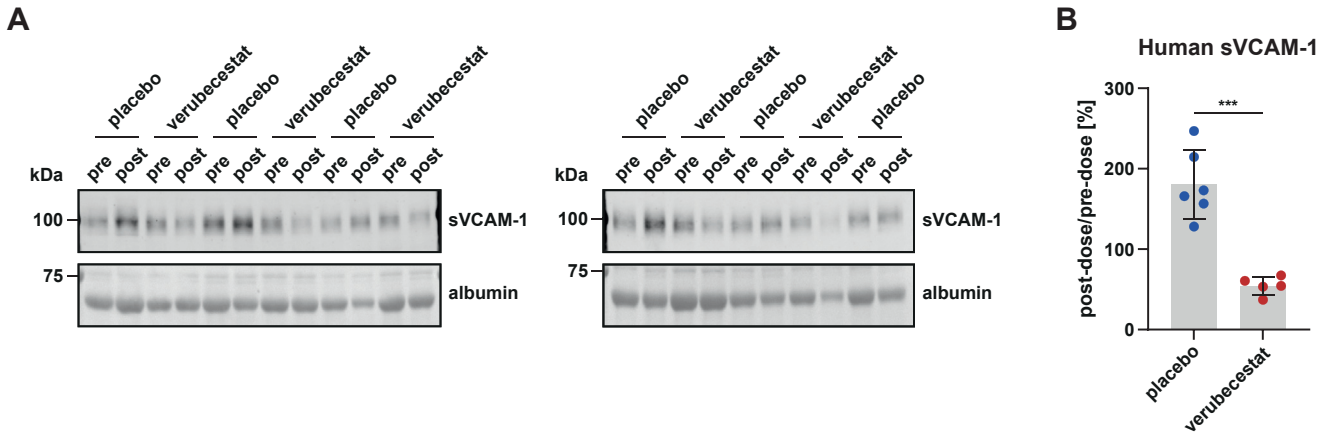

FIG. 5. **Validation of VCAM-1 as BACE2 substrate in human CSF**. *A*, Western blot detection of sVCAM-1 in CSF from participants of a clinical phase 1 study (26). Participants were either treated with placebo (N = 6) or with 550 mg verubecestat (N = 5), and CSF was sampled 2 h before (pre-dose, pre) and 24 h after treatment (post-dose, post). Albumin served as loading control and was visualized by total protein staining. *B*, quantification of Western blot results in *A*. sVCAM-1 signal intensities were first normalized to albumin. Then, the post-dose value for each individual was normalized to the corresponding pre-dose value. Data show mean and SD. Unpaired Student's *t* test. ***$p < 0.001$.

group (Fig. 5*B*). The published data of sAPPβ, $A\beta_{40}$, and $A\beta_{42}$ concentrations (26) showed a comparable decrease in case of sAPPβ (38% remaining relative to pre-dose) and an even stronger reduction for $A\beta_{40}$ and $A\beta_{42}$ (15% and 17% remaining relative to pre-dose, respectively; Supplemental Fig. S4). Although there was no CSF available from individuals treated with a BACE1-selective inhibitor, these results are in agreement with our findings for NHP CSF and clearly indicate that BACE inhibition reduces CSF levels of sVCAM-1 also in humans.

Determination of the BACE2 Cleavage Site in VCAM-1

To identify the BACE2 cleavage site within the VCAM-1 protein sequence, we re-analyzed the NHP CSF of the verubecestat group, similar to Figure 2, where trypsin had been used for protein digestion during proteomic sample preparation. Because trypsin has multiple cleavage sites within the VCAM-1 juxtamembrane sequence, where BACE2 cleavage is expected to occur, we now digested the CSF samples with GluC, which has a different cleavage specificity, generates less peptides and may therefore allow the determination of the BACE2 cleavage site in VCAM-1. Provided that BACE2 cleaves at different peptide bonds in VCAM-1 than GluC, digestion of CSF sVCAM-1 with GluC should result in a peptide near the transmembrane region and with an unspecific C-terminus (*i.e.* not generated by GluC cleavage), indicating the BACE2 cleavage position.

Using the TermineR-based approach, 14 different VCAM-1 peptides were identified (Fig. 6*A*), compared to 10 peptides that were detected in Spectronaut (Fig. 6*B*). Consistent with the tryptic dataset (Fig. 2*B*), the peptides were exclusively localized in the ectodomain and showed an overall decreased abundance upon verubecestat treatment. In both datasets, the same semi-specific peptide with the sequence SKNKVGSQLRSLTL was detected with a C-terminus not resulting from GluC cleavage. The peptide mapped to a region at amino acid positions 670 to 683 which is identical to the human VCAM-1 sequence. The region is only 15 and 16 amino acids away from the transmembrane domain that is annotated to start at position 700 in the NHP sequence and at position 699 in human VCAM-1, respectively (Fig. 6*C*).

These findings were further supported by cleavage of a synthetic VCAM-1 peptide that covered region 673 to 692 of the VCAM-1 sequence. Upon incubation with recombinant BACE2, the synthetic peptide was cleaved at exactly the same position (Fig. 6, *C* and *D*), whereas the synthetic peptide alone remained uncleaved (Fig. 6*D*). Cleavage was almost completely blocked by verubecestat (Fig. 6*D*). Peptide identity in both CSF and the *in vitro* assay was confirmed by MS2 spectra, indicating that in either case the peptide sequence was determined with high confidence (Fig. 6, *E* and *F*). VCAM-1 was cleaved at the peptide bond between leucine at position 683 and aspartate at position 684. The same pattern—C-terminal cleavage at a non-polar amino acid that is followed by a negatively charged one—was also found for a variety of other already published BACE1 and BACE2 cleavage sites (Fig. 6*G* and Supplemental Fig. S5).

As a further control, we re-computed volcano plots for verubecestat, similar to the volcano plot obtained with the trypic digest data in Figure 2*A*, but now using the GluC-digested peptide data either analyzed in Fragpipe (TermineR-based approach) or Spectronaut. With Fragpipe, 630 protein groups were identified with at least two peptides, which is ~30% of protein identifications upon tryptic digest. In Spectronaut, 680 protein groups were detected. The lower sensitivity for protein identification compared to the tryptic digest likely stems from the fact that GluC cleavage results in a considerable amount of neutral and therefore undetectable

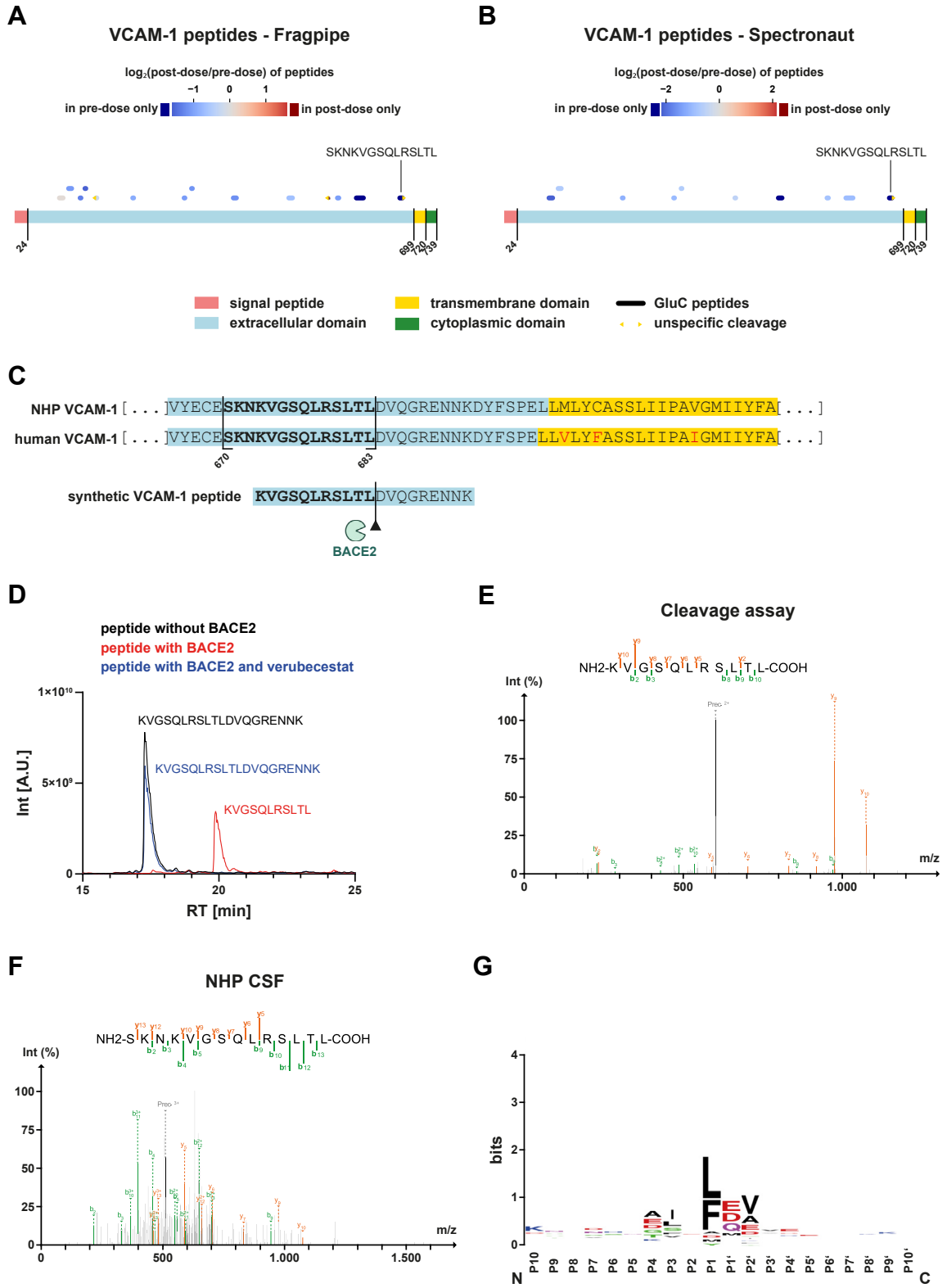

FIG. 6. **Identification of the BACE2 cleavage site in VCAM-1**. *A*, localization and length of sVCAM-1 peptides detected in NHP CSF (N = 4) after GluC digest in a semi-specific TermineR-based search using the Fragpipe software. Peptides were mapped to the UniProt full-length *Macaca fascicularis* VCAM-1 sequence. Protein domain annotations were annotated based on prediction by Phobius. Pre-dose and post-dose CSF from the verubecestat treatment group was analyzed, and peptide LFQ values in the post-dose samples were normalized to the

peptides. Nevertheless, this did not compromise the accuracy with which quantitative changes could be detected for the BACE substrates and substrate candidates also highlighted in Figure 2 (Supplemental Fig. S6). With the exception of CACHD1 and, additionally, with "neural cell adhesion molecule L1-like protein" (CHL1) in Fragpipe, all BACE substrates were detected in both GluC datasets and showed the expected reduction upon verubecestat administration. Albeit the comparison between post- and pre-dose CSF revealed almost similar $\log_2$ fold changes as observed for the verubecestat group versus the IgG RSV control (Fig. 2A), changes in the GluC datasets mostly did not reach FDR significance (Supplemental Fig. S6, *A* and *C*). This is most likely explained by the unpaired comparison of post- and pre-dose samples within one treatment group, which does not account for inter-individual variability. By contrast, when post-dose LFQ values were normalized to the corresponding pre-dose values, BACE substrates showed similar decreases as observed for the tryptic dataset (Supplemental Fig. S6, *B* and *D*).

DISCUSSION

Our study used proteomics to determine how acute treatment with the BACE1-selective inhibitor ATV:BACE1 alters the CSF proteome of NHPs in comparison to verubecestat, a clinically tested small molecule that inhibits both BACE1 and BACE2 (26). While both drugs reduced shedding and release of several BACE1 substrates into CSF, sVCAM-1 was identified and validated to be only reduced in CSF upon inhibition of BACE2 but not BACE1. Our study suggests the use of sVCAM-1 as a biomarker candidate for monitoring BACE2 inhibition for precision medicine in AD clinical trials with BACE inhibitors and for the development of a new generation of BACE1-selective inhibitors. This is further supported by our findings that verubecestat induced a similar decrease in sVCAM-1 levels also in human CSF.

Our study reveals that BACE2 is an *in vivo*-relevant protease for releasing sVCAM-1 into the CSF of NHPs and probably also humans. Inhibition of BACE2 with verubecestat reduced the sVCAM-1 release by about 50%. Either a prolonged BACE2 inhibition is required to fully block VCAM-1 release, or one or several additional proteases contribute to VCAM-1 shedding. In fact, in cell lines ADAM10 and/or ADAM17 contribute to about 50% to the constitutive shedding of VCAM-1 (50, 51), suggesting that either or both ADAMs may mediate the remaining 50% of CSF sVCAM-1 upon BACE2 inhibition in NHPs.

The dependency of sVCAM-1 release on BACE2 but not BACE1, is consistent with a previous study, where an unrelated BACE1/BACE2 inhibitor (MBI-4) reduced sVCAM-1 in NHP CSF by 50% (29). However, in the previous study, it remained unclear whether VCAM-1 shedding was dependent on BACE1 or BACE2, because MBI-4 inhibits both proteases and because no BACE1-selective drug had been used as a control. Our study addressed exactly this specificity question *in vivo* and demonstrates that sVCAM-1 release is BACE2-dependent. Consistent with the previous study using MBI-4, several other substrates showed changes following treatment (SEZ6, IL6ST/gp130, BSG), and our data provides evidence that they are cleaved specifically by BACE1 but not BACE2, as the BACE1-specific inhibitor ATV:BACE1 induced a similar substrate reduction in NHP CSF as verubecestat.

In a previous study using mice and primary murine glial cells, we observed VCAM-1 to be shed by BACE2 (18). While this was seen in cultured glial cells, no change in mouse CSF sVCAM-1 was seen between wild-type and BACE2-deficient mice under constitutive, non-stimulated conditions. This difference between mice and NHPs may be species-specific or result from the chronic BACE2 deficiency in the knock-out mice, versus the acute BACE2 inhibition in the NHPs. Yet, a BACE2 dependency of sVCAM-1 release in mouse CSF was also reported upon mouse brain inflammation after TNF injection (18). Together, these studies demonstrate that sVCAM-1 release into CSF is mediated by BACE2 and that BACE2 contributes to about 50% of sVCAM-1 in NHP CSF.

Similar to the 50% reduction in CSF sVCAM-1 after inhibition of BACE2, we observed that different BACE1 substrates showed distinct degrees of cleavage inhibition after

corresponding pre-dose sample. Peptide coloring represents the $\log_2$ post-dose/pre-dose ratio. Coloring in *dark blue* or *dark red* indicates peptides only detected in pre-dose or post-dose CSF, respectively. Peptides either detected in pre-dose or post-dose CSF, but not in both samples of the same animal (so that calculation of the individual post-dose/pre-dose ratio was not possible), are colored in *dark blue* and *dark red*. Unspecific peptide termini, not resulting from GluC cleavage, are highlighted by *yellow triangles*. *B*, sVCAM-1 peptide mapping for the same samples as in *A* after analysis in Spectronaut. *C*, the semi-specific peptide identified in *A* and *B*, which potentially marks the BACE2 cleavage site, aligns with both *Macaca fascicularis* and human VCAM-1. Ectodomain (*blue*) and transmembrane domain (*yellow*) annotation is based on Phobius prediction (NHP) and UniProt (human), respectively. Amino acids in the human sequence that differ from the NHP VCAM-1 sequence are colored in *red*. In an *in vitro* cleavage assay, a synthetic VCAM-1 peptide was cleaved by BACE2 at the same position as found for CSF sVCAM-1. *D*, total ion chromatograms of the BACE2 cleavage assay of the synthetic VCAM-1 peptide depicted in *C*. Total ion chromatograms are shown for one representative out of two experiments. *E*, MS2 spectrum for the BACE2-cleaved synthetic VCAM-1 peptide. *F*, MS2 spectrum (hyperscore = 24.7) for the semi-specific, potentially BACE2-cleaved VCAM-1 peptide identified in NHP CSF. *G*, sequence logo graphic generated with WebLogo (66) of the amino acid alignment of published BACE1 and 2 substrates around the published cleavage sites (Supplemental Fig. S5). Positively charged amino acids are displayed in *blue*, negatively charged amino acids in *red*, polar amino acids and glycine in *green* or *purple* (glutamine, asparagine), and non-polar amino acids are shown in *black*. The height of the amino acid symbols indicates their frequency at this position.

BACE1 inhibition. For some BACE1 substrates, such as SEZ6 and IL6ST/gp130, the BACE1-cleaved ectodomain in CSF was reduced by both ATV:BACE1 and verubecestat to 50% or less, while for other substrates, such as APLP1, CHL1 and SEZ6L, only mild reductions of less than 50% were observed. The different effect sizes are largely due to the fact that many of the BACE1 substrates are not only cleaved by BACE1, but also by additional proteases, such as ADAM metalloproteases (10). Consequently, ATV:BACE1 and verubecestat only inhibit the BACE1-dependent fraction of substrate cleavage.

VCAM-1 is expressed on the cell surface of different cell types, including specialized epithelial cells, endothelial cells, immune cells, and glial cells, also in the brain, and contributes to immune cell recruitment and adhesion during inflammation (18, 52, 53). VCAM-1 expression is upregulated upon pro-inflammatory stimuli (54), whereas its targeted degradation, for example in a ubiquitin-dependent manner, appears to be an important mechanism to limit inflammatory responses (55). Furthermore, VCAM-1 deletion or antibody blockage counteracted age-associated microglial activation and cognitive impairment induced in young mice when treated with plasma from aged mice (56). Inhibition of VCAM-1 interaction with VLA-4/ITGA4, which is mainly expressed in different immune cells, is also a therapeutic approach in chronic inflammatory diseases (57) and metastatic cancer (58).

Because proteolytic ectodomain shedding, *e.g.* by BACE2, may contribute to membrane protein degradation and homeostasis (10), it is conceivable that VCAM-1 cleavage by BACE2 serves as an additional anti-inflammatory mechanism. In fact, the shedding product sVCAM-1 does not seem to have a pro-inflammatory function, unlike full-length VCAM-1 (56). Given such a potential anti-inflammatory function of BACE2, it appears important for future BACE inhibitors to spare BACE2 and selectively inhibit BACE1, as inflammation plays a central role in AD pathogenesis.

All BACE inhibitors tested to date in advanced clinical trials blocked BACE1 and BACE2 with approximately similar potencies (6). Because inhibition of BACE1 is best suited for a prevention and not a therapy of AD (6), dosing of BACE1-targeted inhibitors may be required over many years for individuals at high risk and would ideally spare BACE2 with its known functions in pigmentation, pancreatic insulin homeostasis, lymphatic vessel maintenance and possibly in VCAM-1-mediated inflammation (59). Development of BACE2-sparing BACE1 inhibitors is ongoing, but no routine assay is yet available for measuring BACE2 target engagement *in vivo*, in particular in CSF, and, thus, for demonstrating a selective inhibition of BACE1 but not BACE2 *in vivo*. As a workaround, BACE2 inhibition is currently functionally monitored in rodents by qualitative scoring of hair depigmentation upon chronic BACE2 inhibition over several weeks (15, 26, 60). However, this assay is not appropriate for pharmacodynamic studies. Our study demonstrates that CSF sVCAM-1 may serve as the BACE2 activity marker suitable for pharmacodynamic studies. The routine use of sVCAM-1 as a BACE2 activity marker requires further optimization, such as the set-up of an immunoassay using an antibody specifically detecting the neo-C-terminus of the BACE2-cleaved sVCAM-1 identified in our study and thus avoiding cross-reactivity with sVCAM-1 generated by other proteases, such as ADAMs, if the cleavage sites are different.

Another translational application besides the development of BACE2-sparing BACE1 inhibitors may be the use of sVCAM-1 to reduce dosing of the currently clinically tested inhibitors to a dose where BACE2 inhibition is minimal, while maintaining a low, but sufficient degree of BACE1 inhibition and Aβ reduction. A previous study (29) together with our one suggests that such an approach may be feasible. While verubecestat (10 mpk) in our study efficiently reduced CSF sVCAM-1 and the BACE1 substrates alike, a 10-fold lower dose of verubecestat (1 mpk) in the previous study did not significantly reduce CSF sVCAM-1 in NHPs, while still decreasing cleavage of the BACE1 substrates SEZ6 and IL6ST by about 25 to 30% (29).

With the pronounced similarity between the NHP and human CSF proteome (29), and supported by the verubecestat-induced reduction of sVCAM-1 in human CSF in this study, it is likely that CSF sVCAM-1 is also a marker for BACE2 activity in the human brain. sVCAM-1 in human CSF can further consistently be detected by LC-MS/MS (61, 62). VCAM-1 levels increase with aging, which was shown in a cognitively healthy cohort spanning an age range of 50 to 100 years (63). The general linkage between VCAM-1 and inflammation and its probable involvement in inflammatory processes associated with AD makes sVCAM-1, beyond its potential suitability to measure BACE2 activity, a potential biomarker candidate for AD-related inflammation (18) and blood-brain barrier dysfunction (64).

sVCAM-1 has also been implicated as a biomarker for cardiovascular disease and for complications in diabetes (53, 54, 59). For these conditions, it will be interesting to see whether BACE2 contributes to sVCAM-1 release to a similar extent as seen in brain and CSF and whether BACE2 is mechanistically involved in pathogenesis.

In summary, our study suggests the use of sVCAM-1 as a biomarker candidate for monitoring BACE2 inhibition for precision medicine in AD clinical trials with BACE inhibitors and for the development of a new generation of BACE1-selective inhibitors.

DATA AVAILABILITY

All data are contained within the manuscript. Python code used in this study is available upon request.

The mass spectrometry proteomics data have been deposited to the ProteomeXchange Consortium *via* the PRIDE (65) partner repository with the dataset identifier PXD056159.

Supplemental data—This article contains supplemental data (15, 26, 28, 42, 67–75)

Acknowledgments—We are grateful for funding by the Deutsche Forschungsgemeinschaft (DFG, German Research Foundation) under Germany's Excellence Strategy within the framework of the Munich Cluster for Systems Neurology (EXC 2145 SyNergy – ID 390857198). This work was further supported by an Alzheimer's association grant (SG-23–1029755 BACE) and the BMBF through grant FKZ161L0214C (ClinspectM).

Author contributions—M. E. K., S. F. L., J. W. L., K. N., Y. J. Y. Z., S. K. T., S. A. M., and J. A. G. investigation; M. E. K. resources; S. F. L., J. W. L., Y. J. Y. Z., S. A. M., and J. A. G. writing–review & editing; S. F. L., J. W. L., Y. J. Y. Z., S. K. T., and J. A. G. validation; S. F. L. supervision; S. F. L. project administration; S. F. L., J. W. L., Y. J. Y. Z., S. K. T., S. A. M., and J. A. G. data curation; S. F. L. conceptualization. J. W. L., Y. J. Y. Z., S. K. T., S. A. M., and J. A. G. formal analysis; S. K. T. writing–original draft; S. K. T. and S. A. M. visualization.

Conflict of interests—The authors declare the following financial interests/personal relationships which may be considered as potential competing interests: The authors declare no competing interests with the exception of Y. Joy Yu Zuchero and Joseph W. Lewcock, who are employees of Denali, and of Matthew E. Kennedy, who is an employee of Merck.

Declaration of generative AI and AI-assisted technologies—No AI or AI-assisted technologies were used in this work.

Abbreviations—The abbreviations used are: Aβ, amyloid β peptide; $A\beta_{40}$, amyloid β peptide 40; $A\beta_{42}$, amyloid β peptide 42; ABC, ammonium bicarbonate; AD, Alzheimer's disease; ADAM10, a disintegrin and metalloproteinase 10; ADAM17, a disintegrin and metalloproteinase 17; AGC, automatic gain control; APLP1, amyloid β precursor like protein 1; APP, amyloid-β precursor protein; ATV, antibody transport vehicle; BACE1, β-site APP cleaving enzyme 1; BACE2, β-site APP cleaving enzyme 2; BSG, basigin; CACHD1, VWFA and cache domain-containing protein 1; CHL1, neural cell adhesion molecule L1-like protein; CNTN2, contactin-2; CSF, cerebrospinal fluid; DDA, data-dependent acquisition; DIA, data-independent acquisition; DTT, dithiothreitol; FDR, false discovery rate; IAA, iodoacetamide; IL6ST, interleukin-6 receptor subunit β; ITGA4, integrin α-4; L1CAM, neural cell adhesion molecule L1; LC-MS/MS, liquid chromatography-coupled tandem mass spectrometry; LFQ, label-free quantification; LRRN1, leucine-rich repeat neuronal protein 1; NHP, non-human primate; PASEF, parallel accumulation-serial fragmentation; QARIP, quantitative analysis of regulated intramembrane proteolysis; RSV, respiratory syncytial virus; sAPPα, soluble APPα; sAPPβ, soluble APPβ; SEZ6, seizure protein 6 homolog; SEZ6L, seizure 6-like protein; SP3, single-pot, solid-phase-enhanced sample preparation; sVCAM-1, soluble VCAM-1; TfR, transferrin receptor; TMEM27, transmembrane protein 27; TNF, tumor necrosis factor; VCAM1, vascular cell adhesion protein 1 (gene name); VCAM-1, vascular cell adhesion protein 1 (protein name); VEGFR3, vascular endothelial growth factor receptor 3; VLA-4, very late antigen-4.

Received September 26, 2024, and in revised form, May 2, 2025
Published, MCPRO Papers in Press, June 4, 2025, https://doi.org/10.1016/j.mcpro.2025.101012

REFERENCES

1. Scheltens, P., De Strooper, B., Kivipelto, M., Holstege, H., Chételat, G., Teunissen, C. E., *et al*. (2021) Alzheimer's disease. *Lancet* **397**, 1577–1590
2. McDade, E., Cummings, J. L., Dhadda, S., Swanson, C. J., Reyderman, L., Kanekiyo, M., *et al*. (2022) Lecanemab in patients with early Alzheimer's disease: detailed results on biomarker, cognitive, and clinical effects from the randomized and open-label extension of the phase 2 proof-of-concept study. *Alzheimer's Res. Ther.* **14**, 191
3. Selkoe, D. J., and Hardy, J. (2016) The amyloid hypothesis of Alzheimer's disease at 25 years. *EMBO Mol. Med.* **8**, 595–608
4. Hampel, H., Vassar, R., De Strooper, B., Hardy, J., Willem, M., Singh, N., *et al*. (2021) The β-secretase BACE1 in Alzheimer's disease. *Biol. Psychiatry* **89**, 745–756
5. Lichtenthaler, S. F., Tschirner, S. K., and Steiner, H. (2022) Secretases in Alzheimer's disease: novel insights into proteolysis of APP and TREM2. *Curr. Opin. Neurobiol.* **72**, 101–110
6. McDade, E., Voytyuk, I., Aisen, P., Bateman, R. J., Carrillo, M. C., De Strooper, B., *et al*. (2021) The case for low-level BACE1 inhibition for the prevention of Alzheimer disease. *Nat. Rev. Neurol.* **17**, 703–714
7. Egan, M. F., Kost, J., Tariot, P. N., Aisen, P. S., Cummings, J. L., Vellas, B., *et al*. (2018) Randomized trial of verubecestat for mild-to-moderate Alzheimer's disease. *N. Engl. J. Med.* **378**, 1691–1703
8. Egan, M. F., Kost, J., Voss, T., Mukai, Y., Aisen, P. S., Cummings, J. L., *et al*. (2019) Randomized trial of verubecestat for prodromal Alzheimer's disease. *N. Engl. J. Med.* **380**, 1408–1420
9. Wessels, A. M., Tariot, P. N., Zimmer, J. A., Selzler, K. J., Bragg, S. M., Andersen, S. W., *et al*. (2020) Efficacy and safety of lanabecestat for treatment of early and mild Alzheimer disease: the AMARANTH and DAYBREAK-ALZ randomized clinical trials. *JAMA Neurol.* **77**, 199–209
10. Lichtenthaler, S. F., Lemberg, M. K., and Fluhrer, R. (2018) Proteolytic ectodomain shedding of membrane proteins in mammals-hardware, concepts, and recent developments. *EMBO J.* **37**, e99456
11. Stutzer, I., Selevsek, N., Esterhazy, D., Schmidt, A., Aebersold, R., and Stoffel, M. (2013) Systematic proteomic analysis identifies beta-site amyloid precursor protein cleaving enzyme 2 and 1 (BACE2 and BACE1) substrates in pancreatic beta-cells. *J. Biol. Chem.* **288**, 10536–10547
12. Rochin, L., Hurbain, I., Serneels, L., Fort, C., Watt, B., Leblanc, P., *et al*. (2013) BACE2 processes PMEL to form the melanosome amyloid matrix in pigment cells. *Proc. Natl. Acad. Sci. U. S. A.* **110**, 10658–10663
13. Esterhazy, D., Akpinar, P., and Stoffel, M. (2012) Tmem27 dimerization, deglycosylation, plasma membrane depletion, and the extracellular Phe-Phe motif are negative regulators of cleavage by Bace2. *Biol. Chem.* **393**, 473–484
14. Rechsteiner, M. P., Floros, X., Boehm, B. O., Marselli, L., Marchetti, P., Stoffel, M., *et al*. (2014) Automated assessment of beta-cell area and density per islet and patient using TMEM27 and BACE2 immunofluorescence staining in human pancreatic beta-cells. *PLoS One* **9**, e98932
15. Schmidt, A., Hrupka, B., van Bebber, F., Sunil Kumar, S., Feng, X., Tschirner, S. K., *et al*. (2024) The Alzheimer's disease-linked protease BACE2 cleaves VEGFR3 and modulates its signaling. *J. Clin. Invest.* **134**, e170550
16. Bennett, B. D., Babu-Khan, S., Loeloff, R., Louis, J. C., Curran, E., Citron, M., *et al*. (2000) Expression analysis of BACE2 in brain and peripheral tissues. *J. Biol. Chem.* **275**, 20647–20651

17. Matafora, V., Farris, F., Restuccia, U., Tamburri, S., Martano, G., Bernardelli, C., *et al*. (2020) Amyloid aggregates accumulate in melanoma metastasis modulating YAP activity. *EMBO Rep.* **21**, e50446
18. Voytyuk, I., Mueller, S. A., Herber, J., Snellinx, A., Moechars, D., van Loo, G., *et al*. (2018) BACE2 distribution in major brain cell types and identification of novel substrates. *Life Sci. Alliance* **1**, e201800026
19. Wang, Z., Xu, Q., Cai, F., Liu, X., Wu, Y., and Song, W. (2019) BACE2, a conditional β-secretase, contributes to Alzheimer's disease pathogenesis. *JCI Insight* **4**, e123431
20. Yeap, Y. J., Kandiah, N., Nizetic, D., and Lim, K. L. (2023) BACE2: a promising neuroprotective candidate for Alzheimer's disease. *J. Alzheimers Dis.* **94**, S159–S171
21. Alić, I., Goh, P. A., Murray, A., Portelius, E., Gkanatsiou, E., Gough, G., *et al*. (2021) Patient-specific Alzheimer-like pathology in trisomy 21 cerebral organoids reveals BACE2 as a gene dose-sensitive AD suppressor in human brain. *Mol. Psychiatry* **26**, 5766–5788
22. Yang, A. C., Vest, R. T., Kern, F., Lee, D. P., Agam, M., Maat, C. A., *et al*. (2022) A human brain vascular atlas reveals diverse mediators of Alzheimer's risk. *Nature* **603**, 885–892
23. He, T., d'Uscio, L. V., and Katusic, Z. S. (2023) BACE2 deficiency impairs expression and function of endothelial nitric oxide synthase in brain endothelial cells. *J. Neurochem.* **166**, 928–942
24. Sáez-Valero, J., and Pérez-González, R. (2023) BACE2 beyond β-processing of APP, its neuroprotective role in cerebrovascular endothelium. *J. Neurochem.* **166**, 887–890
25. Kariolis, M. S., Wells, R. C., Getz, J. A., Kwan, W., Mahon, C. S., Tong, R., *et al*. (2020) Brain delivery of therapeutic proteins using an Fc fragment blood-brain barrier transport vehicle in mice and monkeys. *Sci. Transl. Med.* **12**, eaay1359
26. Kennedy, M. E., Stamford, A. W., Chen, X., Cox, K., Cumming, J. N., Dockendorf, M. F., *et al*. (2016) The BACE1 inhibitor verubecestat (MK-8931) reduces CNS β-amyloid in animal models and in Alzheimer's disease patients. *Sci. Transl. Med.* **8**, 363ra150
27. Neumann, U., Ufer, M., Jacobson, L. H., Rouzade-Dominguez, M. L., Huledal, G., Kolly, C., *et al*. (2018) The BACE-1 inhibitor CNP520 for prevention trials in Alzheimer's disease. *EMBO Mol. Med.* **10**, e9316
28. Pigoni, M., Wanngren, J., Kuhn, P. H., Munro, K. M., Gunnersen, J. M., Takeshima, H., *et al*. (2016) Seizure protein 6 and its homolog seizure 6-like protein are physiological substrates of BACE1 in neurons. *Mol. Neurodegener.* **11**, 67
29. Müller, S. A., Shmueli, M. D., Feng, X., Tüshaus, J., Schumacher, N., Clark, R., *et al*. (2023) The Alzheimer's disease-linked protease BACE1 modulates neuronal IL-6 signaling through shedding of the receptor gp130. *Mol. Neurodegener.* **18**, 13
30. Hughes, C. S., Moggridge, S., Müller, T., Sorensen, P. H., Morin, G. B., and Krijgsveld, J. (2019) Single-pot, solid-phase-enhanced sample preparation for proteomics experiments. *Nat. Protoc.* **14**, 68–85
31. Demichev, V., Messner, C. B., Vernardis, S. I., Lilley, K. S., and Ralser, M. (2020) DIA-NN: neural networks and interference correction enable deep proteome coverage in high throughput. *Nat. Methods* **17**, 41–44
32. The UniProt Consortium. (2022) UniProt: the universal protein knowledgebase in 2023. *Nucleic Acids Res.* **51**, D523–D531
33. Tyanova, S., Temu, T., Sinitcyn, P., Carlson, A., Hein, M. Y., Geiger, T., *et al*. (2016) The Perseus computational platform for comprehensive analysis of (prote)omics data. *Nat. Methods* **13**, 731–740
34. Käll, L., Krogh, A., and Sonnhammer, E. L. (2007) Advantages of combined transmembrane topology and signal peptide prediction–the Phobius web server. *Nucleic Acids Res.* **35**, W429–W432
35. Ivankov, D. N., Bogatyreva, N. S., Hönigschmid, P., Dislich, B., Hogl, S., Kuhn, P. H., *et al*. (2013) QARIP: a web server for quantitative proteomic analysis of regulated intramembrane proteolysis. *Nucleic Acids Res.* **41**, W459–W464
36. Cosenza-Contreras, M., Seredynska, A., Vogele, D., Pinter, N., Brombacher, E., Cueto, R. F., *et al*. (2024) TermineR: extracting information on endogenous proteolytic processing from shotgun proteomics data. *Proteomics* **24**, e2300491
37. Kong, A. T., Leprevost, F. V., Avtonomov, D. M., Mellacheruvu, D., and Nesvizhskii, A. I. (2017) MSFragger: ultrafast and comprehensive peptide identification in mass spectrometry-based proteomics. *Nat. Methods* **14**, 513–520
38. Rappsilber, J., Mann, M., and Ishihama, Y. (2007) Protocol for micro-purification, enrichment, pre-fractionation and storage of peptides for proteomics using StageTips. *Nat. Protoc.* **2**, 1896–1906
39. Colombo, A., Wang, H., Kuhn, P. H., Page, R., Kremmer, E., Dempsey, P. J., *et al*. (2013) Constitutive alpha- and beta-secretase cleavages of the amyloid precursor protein are partially coupled in neurons, but not in frequently used cell lines. *Neurobiol. Dis.* **49**, 137–147
40. Hemming, M. L., Elias, J. E., Gygi, S. P., and Selkoe, D. J. (2009) Identification of beta-secretase (BACE1) substrates using quantitative proteomics. *PLoS One* **4**, e8477
41. Kuhn, P. H., Koroniak, K., Hogl, S., Colombo, A., Zeitschel, U., Willem, M., *et al*. (2012) Secretome protein enrichment identifies physiological BACE1 protease substrates in neurons. *EMBO J.* **31**, 3157–3168
42. Zhou, L., Barão, S., Laga, M., Bockstael, K., Borgers, M., Gijsen, H., *et al*. (2012) The neural cell adhesion molecules L1 and CHL1 are cleaved by BACE1 protease *in vivo*. *J. Biol. Chem.* **287**, 25927–25940
43. Stützer, I., Selevsek, N., Esterházy, D., Schmidt, A., Aebersold, R., and Stoffel, M. (2013) Systematic proteomic analysis identifies β-site amyloid precursor protein cleaving enzyme 2 and 1 (BACE2 and BACE1) substrates in pancreatic β-cells. *J. Biol. Chem.* **288**, 10536–10547
44. Dislich, B., Wohlrab, F., Bachhuber, T., Müller, S. A., Kuhn, P. H., Hogl, S., *et al*. (2015) Label-free quantitative proteomics of mouse cerebrospinal fluid detects β-site APP cleaving enzyme (BACE1) protease substrates *in vivo*. *Mol. Cell Proteomics* **14**, 2550–2563
45. Bateman, R. J., Wen, G., Morris, J. C., and Holtzman, D. M. (2007) Fluctuations of CSF amyloid-beta levels: implications for a diagnostic and therapeutic biomarker. *Neurology* **68**, 666–669
46. Huang, Y., Potter, R., Sigurdson, W., Santacruz, A., Shih, S., Ju, Y. E., *et al*. (2012) Effects of age and amyloid deposition on Aβ dynamics in the human central nervous system. *Arch. Neurol.* **69**, 51–58
47. Li, J., Llano, D. A., Ellis, T., LeBlond, D., Bhathena, A., Jhee, S. S., *et al*. (2012) Effect of human cerebrospinal fluid sampling frequency on amyloid-β levels. *Alzheimers Dement.* **8**, 295–303
48. Lucey, B. P., Gonzales, C., Das, U., Li, J., Siemers, E. R., Slemmon, J. R., *et al*. (2015) An integrated multi-study analysis of intra-subject variability in cerebrospinal fluid amyloid-β concentrations collected by lumbar puncture and indwelling lumbar catheter. *Alzheimer's Res. Ther.* **7**, 53
49. Lucey, B. P., Fagan, A. M., Holtzman, D. M., Morris, J. C., and Bateman, R. J. (2017) Diurnal oscillation of CSF Aβ and other AD biomarkers. *Mol. Neurodegener.* **12**, 36
50. Garton, K. J., Gough, P. J., Philalay, J., Wille, P. T., Blobel, C. P., Whitehead, R. H., *et al*. (2003) Stimulated shedding of vascular cell adhesion molecule 1 (VCAM-1) is mediated by tumor necrosis factor-alpha-converting enzyme (ADAM 17). *J. Biol. Chem.* **278**, 37459–37464
51. Singh, R. J., Mason, J. C., Lidington, E. A., Edwards, D. R., Nuttall, R. K., Khokha, R., *et al*. (2005) Cytokine stimulated vascular cell adhesion molecule-1 (VCAM-1) ectodomain release is regulated by TIMP-3. *Cardiovasc. Res.* **67**, 39–49
52. Karlsson, M., Zhang, C., Mear, L., Zhong, W., Digre, A., Katona, B., *et al*. (2021) A single-cell type transcriptomics map of human tissues. *Sci. Adv.* **7**, eabh2169
53. Brishti, M. A., Raghavan, S., Lamar, K., Singh, U. P., Collier, D. M., and Leo, M. D. (2023) Diabetic endothelial cell glycogen synthase kinase 3beta activation induces VCAM1 ectodomain shedding. *Int. J. Mol. Sci.* **24**, 14105
54. Troncoso, M. F., Ortiz-Quintero, J., Garrido-Moreno, V., Sanhueza-Olivares, F., Guerrero-Moncayo, A., Chiong, M., *et al*. (2021) VCAM-1 as a predictor biomarker in cardiovascular disease. *Biochim. Biophys. Acta Mol. Basis Dis.* **1867**, 166170
55. Li, Y., Huang, X., Guo, F., Lei, T., Li, S., Monaghan-Nichols, P., *et al*. (2020) TRIM65 E3 ligase targets VCAM-1 degradation to limit LPS-induced lung inflammation. *J. Mol. Cell Biol.* **12**, 190–201
56. Yousef, H., Czupalla, C. J., Lee, D., Chen, M. B., Burke, A. N., Zera, K. A., *et al*. (2019) Aged blood impairs hippocampal neural precursor activity and activates microglia *via* brain endothelial cell VCAM1. *Nat. Med.* **25**, 988–1000
57. Yusuf-Makagiansar, H., Anderson, M. E., Yakovleva, T. V., Murray, J. S., and Siahaan, T. J. (2002) Inhibition of LFA-1/ICAM-1 and VLA-4/VCAM-1 as a therapeutic approach to inflammation and autoimmune diseases. *Med. Res. Rev.* **22**, 146–167

58. VanHeyst, K. A., Choi, S. H., Kingsley, D. T., and Huang, A. Y. (2022) Ectopic tumor VCAM-1 expression in cancer metastasis and therapy resistance. *Cells* **11**, 3922
59. Singh, V., Kaur, R., Kumari, P., Pasricha, C., and Singh, R. (2023) ICAM-1 and VCAM-1: gatekeepers in various inflammatory and cardiovascular disorders. *Clin. Chim. Acta* **548**, 117487
60. Shimshek, D. R., Jacobson, L. H., Kolly, C., Zamurovic, N., Balavenkatraman, K. K., Morawiec, L., *et al*. (2016) Pharmacological BACE1 and BACE2 inhibition induces hair depigmentation by inhibiting PMEL17 processing in mice. *Sci. Rep.* **6**, 21917
61. [preprint] Lourbopoulos, A., Müller, S. A., Jocher, G., Wick, M., Plesnila, N., and Lichtenthaler, S. F. (2024) An improved method for sampling and quantitative protein analytics of cerebrospinal fluid of single mice. *bioRxiv*. https://doi.org/10.1101/2024.06.18.599559
62. Pesamaa, I., Muller, S. A., Robinson, S., Darcher, A., Paquet, D., Zetterberg, H., *et al*. (2023) A microglial activity state biomarker panel differentiates FTD-granulin and Alzheimer's disease patients from controls. *Mol. Neurodegener.* **18**, 70
63. Li, G., Shofer, J. B., Petrie, E. C., Yu, C. E., Wilkinson, C. W., Figlewicz, D. P., *et al*. (2017) Cerebrospinal fluid biomarkers for Alzheimer's and vascular disease vary by age, gender, and APOE genotype in cognitively normal adults. *Alzheimer's Res. Ther.* **9**, 48
64. Cano, A., Turowski, P., Ettcheto, M., Duskey, J. T., Tosi, G., Sánchez-López, E., *et al*. (2021) Nanomedicine-based technologies and novel biomarkers for the diagnosis and treatment of Alzheimer's disease: from current to future challenges. *J. Nanobiotechnol.* **19**, 122
65. Perez-Riverol, Y., Bai, J., Bandla, C., García-Seisdedos, D., Hewapathirana, S., Kamatchinathan, S., *et al*. (2022) The PRIDE database resources in 2022: a hub for mass spectrometry-based proteomics evidences. *Nucleic Acids Res.* **50**, D543–D552
66. Crooks, G. E., Hon, G., Chandonia, J. M., and Brenner, S. E. (2004) WebLogo: a sequence logo generator. *Genome Res.* **14**, 1188–1190
67. Vassar, R., Bennett, B. D., Babu-Khan, S., Kahn, S., Mendiaz, E. A., Denis, P., *et al*. (1999) Beta-secretase cleavage of Alzheimer's amyloid precursor protein by the transmembrane aspartic protease BACE. *Science* **286**, 735–741
68. Kuhn, P. H., Marjaux, E., Imhof, A., De Strooper, B., Haass, C., and Lichtenthaler, S. F. (2007) Regulated intramembrane proteolysis of the interleukin-1 receptor II by alpha-, beta-, and gamma-secretase. *J. Biol. Chem.* **282**, 11982–11995
69. Hogl, S., Kuhn, P.-H., Colombo, A., and Lichtenthaler, S. F. (2011) Determination of the proteolytic cleavage sites of the amyloid precursor-like protein 2 by the proteases ADAM10, BACE1 and γ-secretase. *PLOS ONE* **6**, e21337
70. Wong, H.-K., Sakurai, T., Oyama, F., Kaneko, K., Wada, K., Miyazaki, H., *et al*. (2005) Beta subunits of voltage-gated sodium channels are novel substrates of beta-site amyloid precursor protein-cleaving enzyme (BACE1) and gamma-Secretase. *J. Biol. Chem.* **280**, 23009–23017
71. Rudan Njavro, J., Klotz, J., Dislich, B., Wanngren, J., Shmueli, M. D., Herber, J., *et al*. (2020) Mouse brain proteomics establishes MDGA1 and CACHD1 as in vivo substrates of the Alzheimer protease BACE1. *FASEB J.* **34**, 2465–2482
72. Willem, M. (2016) Proteolytic processing of Neuregulin-1. *Brain Res. Bull.* **126**, 178–182
73. Hu, X., He, W., Diaconu, C., Tang, X., Kidd, G. J., Macklin, W. B., *et al*. (2008) Genetic deletion of BACE1 in mice affects remyelination of sciatic nerves. *FASEB J.* **22**, 2970–2980
74. Kitazume, S., Tachida, Y., Oka, R., Kotani, N., Ogawa, K., Suzuki, M., *et al*. (2003) Characterization of α2,6-sialyltransferase cleavage by Alzheimer's β-secretase (BACE1). *J. Biol. Chem.* **278**, 14865–14871
75. Lichtenthaler, S. F., Dominguez, D.-I., Westmeyer, G. G., Reiss, K., Haass, C., Saftig, P., *et al*. (2003) The cell adhesion protein P-selectin glycoprotein ligand-1 is a substrate for the aspartyl protease BACE1. *J. Biol. Chem.* **278**(49), 48713–48719